EFFECTS OF ANODIZATION ELECTROLYTE ON THE FORMATION OF NANOPOROUS TITANIUM OXIDE (TiO$_2$) FOR PHOTOCATALYTIC APPLICATION

LEONG MEI YEE

A project report submitted in partial fulfilment of the requirements for the award of Bachelor of Engineering (Hons.) Materials and Manufacturing Engineering

Lee Kong Chian Faculty of Engineering and Science
Universiti Tunku Abdul Rahman

August 2017

DECLARATION

I hereby declare that this project report is based on my original work except for citations and quotations which have been duly acknowledged. I also declare that it has not been previously and concurrently submitted for any other degree or award at UTAR or other institutions.

Signature : _____

Name : Leong Mei Yee

ID No. : 13UEB00687

Date : 18th September 2017

APPROVAL FOR SUBMISSION

I certify that this project report entitled **"EFFECTS OF ANODIZATION ELECTROLYTE ON THE FORMATION OF NANOPOROUS TITANIUM OXIDE (TiO₂) FOR PHOTOCATALYTIC APPLICATION"** was prepared by **LEONG MEI YEE** has met the required standard for submission in partial fulfilment of the requirements for the award of Bachelor of Engineering (Hons.) Materials and Manufacturing Engineering at Universiti Tunku Abdul Rahman.

Approved by,

Signature   :   _____

Supervisor   :   Dr Ng Chai Yan

Date   :   18th September 2017

Signature   :   -

Co-Supervisor :   -

Date   :   -

The copyright of this report belongs to the author under the terms of the copyright Act 1987 as qualified by Intellectual Property Policy of Universiti Tunku Abdul Rahman. Due acknowledgement shall always be made of the use of any material contained in, or derived from, this report.

ACKNOWLEDGEMENTS

I wish to express my sincere gratitude by using this golden opportunity to everyone who had lend me a helping hand in completing this entire project.

First of all, I would like to sincerely thank my supervisor, Dr Ng Chai Yan for her guidance, encouragement, invaluable advice and constructive criticism throughout this whole project. I am really thankful for the opportunity to conduct my project under her supervision.

Other than that, I would like to extend my gratefulness to all the lab assistants of both Universiti Tunku Abdul Rahman Sungai Long and Kampar campuses for their assistance in operating equipment for various analytical tests. Finally, I would like to thank my parents for showing their sacrifice and support both mentally and physically, without them I would not be able to complete my project efficiently.

ABSTRACT

Titanium oxide (TiO$_2$) is the most commonly known photocatalyst for decomposing organic pollutants by changing light energy to dependable effective chemical energy. Electrochemical anodization method was used to prepare nanoporous TiO$_2$ on Ti substrate to increase its photocatalytic efficiency. In this work, Ti was anodised in various concentrations of NH$_4$F (0.1, 0.2, 0.3 and 0.4 g) with the addition of EG and KOH. The effects of electrolyte concentration on the morphological, structural and photocatalytic properties of the samples were investigated. Nanopores were present after anodization. The smallest pore wall thickness was measured after anodizing the samples in electrolyte containing 0.3 g of NH$_4$F (~8.0 nm). The sample also has the highest pore density which can be judged by its small pore diameter (~21.7 nm) and thin pore walls. The EDX spectrum showed significant Ti and O peaks which indicates the formation of oxide layer after anodization. XRD results showed that the annealed sample anodized with 0.3 g of NH$_4$F has the highest intensity and narrow anatase peaks among all samples. TiO$_2$ nanostructures must attain two characteristics to exhibit high photocatalytic performance which is a large surface area for absorbing substrates and high crystallinity to minimize the rate of photoexcited e$^-$/h$^+$ recombination. The sample anodized by using 0.3 g of NH$_4$F fulfilled both of the requirements. Therefore, it has showed the best photocatalytic efficiency (~23%) among all samples.

TABLE OF CONTENTS

CHAPTER

LIST OF TABLES

LIST OF FIGURES

LIST OF SYMBOLS / ABBREVIATIONS

AOP	Advanced Oxidation Process
CB	Conduction band
MB	Methylene blue
UV	Ultraviolet
UV-Vis	UV–visible spectrophotometer
VB	Valance band

CHAPTER 1

INTRODUCTION

1.1   General Introduction

One of the most commonly used photocatalyst today is titanium oxide (TiO_2). TiO_2 is well known for decomposing organic pollutants by changing light energy to dependable effective chemical energy. In 1972, photosensitization effect was discovered by Honda and Fujishima (1972). It is found that TiO_2 electrode was able to electrolyse water to H_2 and O_2 using TiO_2 anode and a platinum counter electrode (Fujihira, Satoh and Osa, 1981). Although TiO_2 is known for its substantial prospective as a photocatalyst, the low photocatalytic efficiency of compact TiO_2 surfaces obstructs its role in the photocatalytic oxidation technology. To increase its photocatalytic efficiency, investigation shows that nanoporous TiO_2 layer has high potential of achieving this purpose depending on its huge surface area and large pore capacity (Prabhu et al., 2014).

In this work, electrochemical anodization method was used to prepare nanoporous TiO_2 on Ti substrate. The photocatalytic properties of nanoporous TiO_2 layers were inspected by disintegrating aqueous methylene blue (MB) solution using ultraviolet (UV) light (Dikici et al., 2015). When TiO_2 is in intimate contact with an aqueous solution of the pollutants, TiO_2 develops a redox environment which can effectively oxidize the pollutants into nontoxic substances such as carbon dioxide (CO_2) and water (H_2O) (Bard, 1979).

Anodization was completed through self-organizing conditions which is able to be tuned to highly arranged arrays of firmly packed vertically coordinated nanopores (Tighineanu et al., 2010). In order to fully utilize the photocatalytic properties of TiO_2, high temperature annealing is essential to convert TiO_2 from its amorphous phase to crystalline forms (Chen and Mao, 2007). TiO_2 is categorized into few different crystalline structures which are rutile, anatase and brookite. Anatase was found to be more effective photocatalytically and metastable structure in comparison to rutile and brookite which are in chemically stable phases. (Harikishore et al., 2014). This crystallographic transformation is depending on the annealing temperature (Sul et al., 2001).

1.2   Importance of the Study

In recent years, water contamination is becoming a critical environmental issue and it is causing destruction on a global scale (Anpo, 2017). The commercial and scientific communities have been attempting to tackle this issue by using a number of processes including chlorination, ozonation, filtration or exposed to radiation. However, these methods soon became unfavourable due to the costly operation process and generation of toxic by-products which are mutagenic and carcinogenic to human health (Linsebigler, Lu and Yates, 1995; Venieri et al., 2014). In order to tackle these problems, the research in photocatalysis is important.

1.3   Problem Statement

As mentioned in Section 1.1, electrochemical anodization of Ti is a relatively simple process to engineer highly ordered TiO_2 porous or tubular structures. In anodization, the electrolyte plays an important role because the morphology and composition of the nanopores are directly influenced by the electrolyte system used. The fabrication of TiO_2 nanoporous arrays was achieved by anodizing Ti metal in aqueous hydrofluoric acid (HF) electrolyte in earlier research (Krengvirat et al., 2013). In fluoride-containing electrolytes, dissolution of TiO_2 happens because of preferable formation of titanium hexafluoride ($[TiF_6]^{2-}$) (Macák, Tsuchiya and Schmuki, 2005). As a result, the porous titania produced only obtained a maximum thickness of approximately 500 nm due to high chemical dissolution (Ali et al., 2011; Tsuchiya and Schmuki, 2004). The presence of F ions is required for dissolution of titania for the pore formation. However, this prevents the thickening of the porous layer when the pH is low which causes high dissolution rate (Macák, Tsuchiya and Schmuki, 2005).

Later studies have been attempted to achieve better pore morphology and improve the thickness of nanoporous oxide films growth on Ti by using organic solvents such as formamide (FA), dimethyl sulfoxide (DMSO), ethylene glycol (EG) and N-methylformamide (NMF) (Nyein et al., 2016). The results showed that EG containing ammonium fluoride (NH_4F) instead of HF possesses great potential for the formation of better nanoporous arrays (Macák, Tsuchiya and Schmuki, 2005). The reduction of acidity causes a decrease in chemical dissolution which forms highly ordered nanoporous arrays with thicker oxide films (Krengvirat et al., 2013). However, there is a great increase in anodization time to obtain the desired result which is limited for practical applications. To solve this problem, KOH was added to the electrolyte.

This addition increases the pH of electrolyte up to approximately 9, which reduces chemical dissolution to form highly ordered nanoporous arrays in a shorter time (Nyein et al., 2016).

1.4   Aims and Objectives

The aim of this project is to study the effects of anodization electrolyte on the formation of nanoporous TiO_2 for photocatalytic application.

The objectives of this study are:

(i)   To determine the effects of the concentration of electrolyte on the anodic growth of nanoporous TiO_2.

(ii)   To investigate the morphological and structural properties of nanoporous TiO_2.

(iii)   To correlate the morphological and structural properties of nanoporous TiO_2 with its photocatalytic properties.

1.5   Scope and Limitation of the Study

This study covers the effects of the concentration of anodization electrolyte on the formation of nanoporous TiO_2. By altering the electrolyte concentration, the morphology of the nanostructures formed will be different. The change on the morphology affects the photocatalytic performances. This study only covers one of the anodizing parameters which is the concentration of electrolyte. Other parameters including type of electrolyte, applied voltage, pH and duration time are not discussed here (Sul et al., 2001).

1.6   Contribution of the Study

Prior to this research, many study reported the effects of anodization electrolyte on the formation of nanoporous TiO_2 for photocatalytic application. However, no research has been done on the effects of anodization electrolyte that consists of KOH, NH_4F and EG on the formation of nanoporous TiO_2 for photocatalytic application. In this study, the effects of the concentration of electrolyte on the anodic growth of nanoporous TiO_2 was done by altering the concentration of NH_4F in the electrolyte. Besides, the morphological and structural properties of the samples were also investigated in this study.

1.7   Outline of the Report

Chapter 1 shows the overview of this research. Chapter 2 reviews the details of related work which includes:

(i)   Research background on photocatalytic process and materials.

(ii) TiO_2 nanostructures.

(iii) TiO_2 synthetization methods.

Chapter 3 elaborates the experimental procedures of fabricating nanoporous TiO_2 films and characterisation analysis done on the samples while chapter 4 includes the results and discussion of the TiO_2 films produced by anodization. The final chapter shows the conclusion and future recommendations of this study.

CHAPTER 2

LITERATURE REVIEW

2.1   Introduction

The review of the photocatalytic properties, nanostructures, and synthetization methods for TiO_2 nanostructures are discussed in this chapter. Photocatalytic process is the primary concern in this research and its requirements are briefed. In addition, the TiO_2 nanostructures of nanospheres, nanotubes and nanopores are assessed in this chapter. Lastly, the synthesis methods of sol-gel, hydrothermal, and anodization are also explored.

2.2   Photocatalytic Process

Photocatalytic process is meant to initiate redox reactions when irradiated semiconductors are present as a catalyst. It produces reactive oxidizing species that leads to photocatalytic transformation pollutants (FUJISHIMA, ZHANG and TRYK, 2008). At least two events must happen concurrently to produce reactive oxidizing species. First involves the oxidizing dissociative adsorbed H_2O by photogenerated holes. Next is reducing an electron acceptor through photoexcited electrons. These cause the production of a superoxide radical anion and hydroxyl (Suh et al., 2010).

As shown in Figure 2.1, the function of semiconductor energy band gap possessing greater energy is to emit light inside the semiconductor. This causes the absorbent material on its surface to react through a redox reaction known as photocatalytic reaction. It is based on solar energy absorption in the band gap of semiconductor with photogenerated electron transfer (FUJISHIMA, ZHANG and TRYK, 2008).
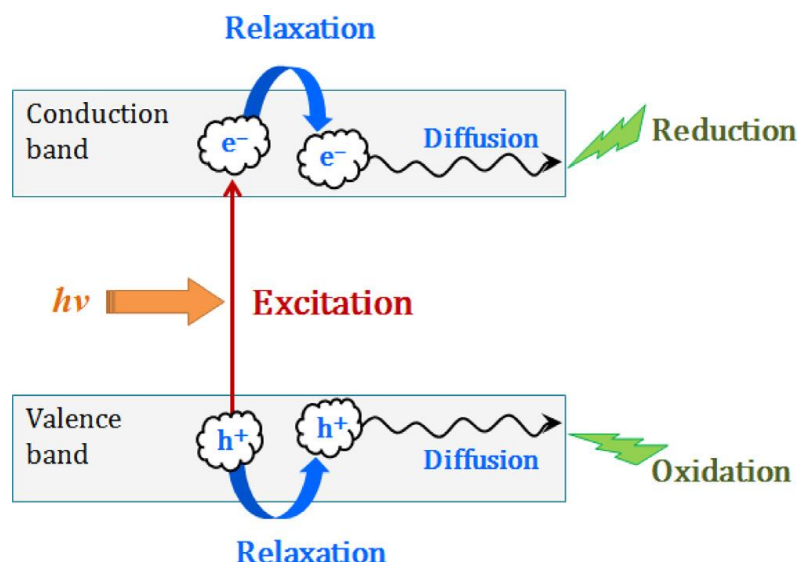
Figure 2.1: Schematic Illustration of the Formation of Photo-Induced Charge Carriers (e^-/ h^+) on Absorption of UV Light (Lee and Park, 2013)

Photocatalysis was discovered through rapid research development in "Advanced Oxidation Process (AOP)" as a method for water purification. AOP is a method that uses a range of technologies to increase oxidation power and mineralization of organic compounds by generating highly reactive transitory species on-site (Esplugas et al., 2002; Pera-Titus et al., 2004). Heterogeneous photocatalysis employing semiconductor catalysts stood out among all AOPs as it is capable of degrading various ambiguous refractory organics into degradable compounds and are gradually mineralized to non-toxic substances like CO_2 and H_2O (Malato et al., 2009).

One of a few favourable choices to tackle water pollution and shortage using a number of different processes before discovering photocatalysis is treating urban wastewater for future activities. This method is highly anticipated as reusing wastewater will produce cleaner water resource. However, this usually links with the existence of suspended solids, bacteria and organic compounds in the water that are costly and complicated to eliminate (Viessman and Hammer, 1998). Other than that, technologies like adsorption and coagulation does not completely solve the problem as they merely just transfer the pollutants to other phases and still remains in the water (Padmanabhan et al., 2006). Table 2.1 shows the comparison between photocatalytic system and other existing water treatment methods. Therefore, based on the evidence above, photocatalysis is more preferable compared to other conventional methods (Lee and Park, 2013).

Table 2.1: Comparing Advantages and Disadvantages of Photocatalytic System and the Existing Water Treatment Methods (Lee and Park, 2013)

	Advantages	Disadvantages
Biological Treatment Technique	- High reliability - High load operation	- Efficiency of processing difficulty securing stable - High level of sludge - Operating management requires expertise
Coagulation/ Precipitation	- High efficiency in processing - Low sites	- Excessive sludge - Difficult to maintain
Fenton Technology	- Wide coverage - Treatment process is simple and easy to manage - Effective coloured discolouration of wastewater	- High operating cost - Remove the equipment needed iron salts
Photocatalytic Advanced Oxidation Technology	- Non-biodegradable waste water treatment is possible - Low operational and installation cost - Sludge treatment cost do not occur - Simple pre-processing - Less area is linked with the existence treatment facilities	- Limited lamp life when UV lamp is used - Photocatalyst recovery facility when powder is used

2.3 Photocatalytic Materials

Traditionally popular visible-light photocatalysts consists of cadmium sulphide (CdS), gallium phosphide (GaP), cadmium selenide (CdSe), tungsten (VI) oxide (WO_3) and iron (III) oxide (Fe_2O_3). They all soon became unfavourable due to their limitation. A few characteristics is needed to extend the role of photocatalyst in water purification such as (Chong et al., 2010):

- ambient operating pressure and temperature
- complete mineralization without secondary pollution
- affordable

CdS and GaP forms toxic products when degrading which cause environmental pollution and carcinogenic to human health (Malato et al., 2009). Furthermore, upon illumination, CdS and CdSe are unstable (Choi et al., 2008) while WO_3 and Fe_2O_3 has

low activity (Jang, Kim and Lee, 2012). UV-active oxides are improvised to operate as photocatalysts by substitutional doping with metals like vanadium (V), iron (Fe) or manganese (Mn) (Zou et al., 2001) or forming compounds with nitrogen (N), carbon (C) and sulfur (S) (Hwang et al., 2005). However, these doped materials showed only minimal results. TiO_2 is found to be most active even after repeated catalytic cycles within the photon energy of 300 nm < l < 390 nm (Chong et al., 2010).

2.3.1   Titanium oxide (TiO₂)

TiO_2 based photocatalysts are applied widely to control environmental pollution. TiO_2 photocatalysis is a photo-induced charge separation occurrence on its surface and very high reactive oxygen species. It induces organic mineralization and microbial inactivation without causing any secondary pollution (Zhang and Yu, 2003).

The decomposition is commonly an oxidation depending on the valance band (VB) of photocatalyst for polluted materials. When VB holes have larger oxidative power and electrochemical potential with higher positivity respect to normal hydrogen electrode (NHE) potential, oxidation reaction improves. The band gap of TiO_2 is usually ranging from 3.0 to 3.2 eV and possessing a wavelength around 400 nm. Therefore, photo-reaction will begin when UV light irradiates with a wavelength lower than 400 nm (Suh et al., 2010).

The photon energy generated is similar to 30,000 $^{\circ}C$ of thermal energy. Therefore, it is possible to attain heat higher than 30,000 $^{\circ}C$ on its surface when TiO_2 is irradiates with UV light below 400 nm. This oxidizes all materials causing organic compounds to decompose into H_2O and CO_2 (Hernández-Alonso et al., 2009). Figure 2.2 shows the elimination of pollutants by photoinduced charge carriers (e^-/h^+) (Lee and Park, 2013).
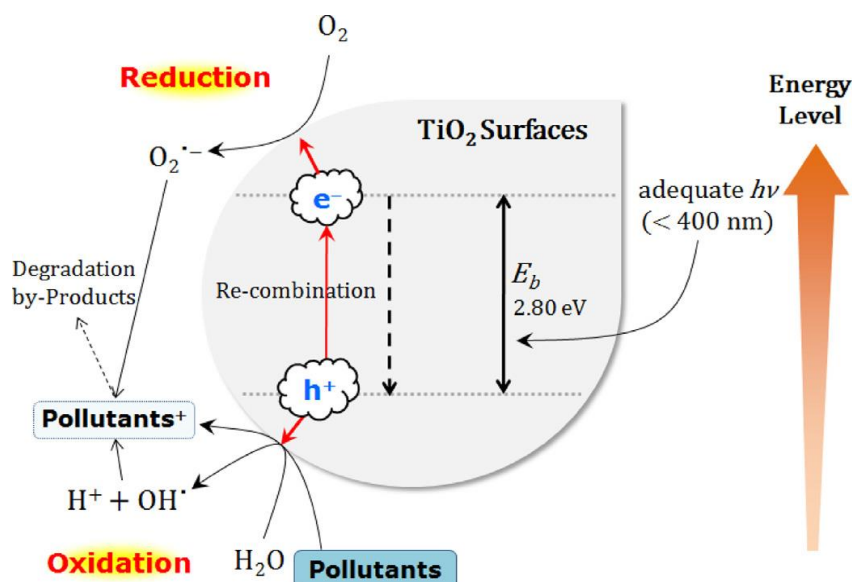
Figure 2.2: Schematic Illustration on Removal of Pollutants by the Photo-Induced Charge Carriers (e^-/h^+) in a Semiconductor TiO_2 Particle Surfaces (Lee and Park, 2013)

Based on Figure 2.2, the photo-induced electrons in the conduction band (CB) will join the reduction processes when surface of the TiO_2 catalysts suspended in water irradiates with UV light. It reacts with dissolved O_2 in air to produce superoxide radical anions ($O_2\cdot^-$). OH· (hydroxide radicals) forms when photo-induced holes in the VB diffuse on the TiO_2 surface reacting with adsorbed H_2O molecules (Hagfeldt and Graetzel, 1995; Banerjee, Joo and Min, 2012). This mechanism is shown in Figure 2.2 where e^-_{TR} and h^+_{TR} represents trapped VB electron and CB hole on surface (Lee and Park, 2013).

Next, TiO_2 can be mass produced as it is highly available, affordable and can be easily fabricated in a laboratory. TiO_2 is very stable and possess strong resistance against acids and alkalis (Zhou, Ding and Wu, 2013). The charge-pair on the TiO_2 surface reacts under irradiation with solid lattice ions, therefore it will not experience photo-corrosion degradation. The TiO_2 photocatalytic system has been certified due to its strong photocatalytic properties. Table 2.2 lists the non-biodegradable organic pollutants degraded by the TiO_2 photocatalytic system. All these good properties render the TiO_2 photocatalytic system as a promising technology for degrading organic pollutants in water treatment (Lee and Park, 2013).

Table 2.2: Non-Biodegradable Organic Pollutants Degradable Using TiO_2 Photocatalytic System (Lee and Park, 2013)

CH_3CHO, Acetaldehyde	CCl_4, Carbon tetrachloride	$(HO_2CCH_2)_2NCH_2CH_2N(CH_2CO_2H)_2$, Ethylenediaminetetraacetic acid (EDTA)	$C_6H_5NO_2$, Nitrobenzene
R–CHO Aldehyde	$CHCl_3$ Chloroform	R–O–R′ Ether	$C_3H_5(NO_3)_3$ Nitroglycerine
CH_3COOH Acetic acid	CH_3Cl Chloromethane	HCHO Formaldehyde	H_2NNO_2 Nitroamine
CH_3COCH_3 Acetone	$C_{10}H_7Cl$ Chloronaphthalene	HCOOH Formic acid	$C_{12}Cl_xH_{10-x}$ Polychlorinated biphenyl (PCBs)
C_3H_4O Acrolein	$C_6H_4(CH_3)OH$ Cresol	C_6Cl_6 Hexachlorobenzene	$C_{14}H_{10}$ Phenanthrene
$C_3H_4O_2$ Acrylic acid	$Cl_2C_6H_3OH$ Dichlorophenol	N_2H_4 Hydrazine	C_6H_5OH Phenol
C_6H_6 Benzene	$C_{12}H_{10}Cl_2N_2$ Dichlorobenzidine	$C_8H_6O_4$ Isophthalic acid	$Cl_2C=CCl_2$ Tetrachloroethylene
C_6H_5COOH Benzoic acid	$(CH_3)_2NNO$ Dimethylnitrosamine	CH_2Cl_2 Methylene Chloride	$C_6H_5CH_3$ Toluene
$CH_3CH_2CH_2COOH$ Butyric acid	$C_{12}H_4Cl_4O_2$ Dioxin	$C_{10}H_8$ Naphthalene	$C_6H_4(CH_3)_2$ Xylene

2.4   Crystalline Phases of TiO_2

Crystalline structures of TiO_2 include rutile, brookite and anatase (Bonnet et al., 2015). All three polymorphs are able to be synthesised in the laboratory. All three forms are able to form TiO_6 octahedra by coordinating titanium (Ti^{4+}) atoms to six oxygen (O^{2-}) atoms. Table 2.3 shows the crystal structure data of TiO_2. Anatase has a more active photocatalytic structure and metastable compared to the chemically stable brookite and rutile (Harikishore et al., 2014).

Table 2.3: The Crystal Structure Data of TiO_2 (Sugiyama and Takéuchi, 1991)

Properties	Rutile	Anatase	Brookite
Crystal structure	Tetragonal	Tetragonal	Orthorhombic
Lattice constant (Å)	$a = 4.5936$ $c = 2.9587$	$a = 3.784$ $c = 9.515$	$a = 9.184$ $b = 5.447$ $c = 5.154$
Space group	$P4_2/mnm$	$I4_1/amd$	Pbca
Molecule (cell)	2	2	4
Volume/ molecule ($Å^3$)	31.2160	34.061	32.172
Density (g cm^{-3})	4.13	3.79	3.99
Ti–O bond length (Å)	1.949 (4) 1.980 (2)	1.937(4) 1.965(2)	1.87–2.04
O–Ti–O bond angle	81.2° 90.0°	77.7° 92.6°	77.0°–105°

2.4.1   Titanium oxide (TiO_2)

Rutile possesses tetragonal structure which contains 6 atoms per unit cell (Figure 2.3) (Gupta and Tripathi, 2012). Octahedra share edges at (001) planes in rutile to obtain

tetragonal structure. The band gap of rutile is reported to be approximately 3.0 eV. This phase of TiO_2 is stable at most temperatures and pressure up to 60 kbar (Zhao, Chang and Zhai, 2005). After attaining a certain particle size, other crystalline structures are able to convert into rutile. Rutile becomes more stable compared to anatase for particle sizes larger than 14 nm. Despite the stability, its activity as a photocatalyst is weak. However, research shown rutile can be active or inactive relying on preparation conditions (Sclafani, Palmisano and Schiavello, 1990).
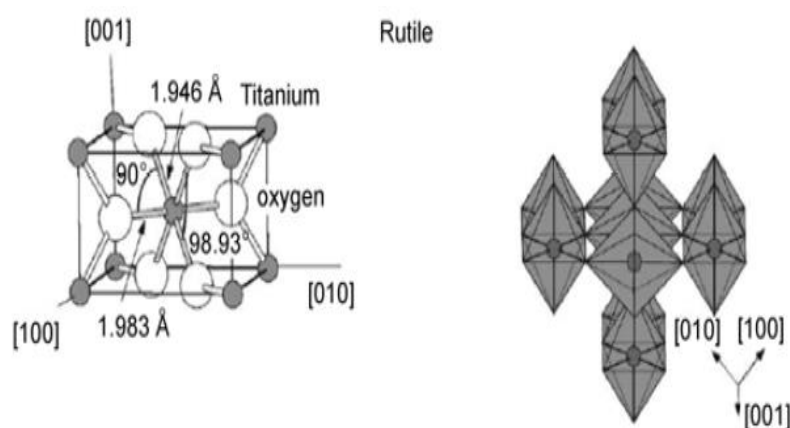
Figure 2.3: Crystal Structure of Rutile Phase TiO_2 (Gupta and Tripathi, 2012)

2.4.2 Brookite

Brookite is categorized in the orthorhombic crystal system with a band gap of approximately 3.2 eV which could be higher or lower compared to anatase. Its unit cell is made up of octahedra, each with a Ti atom at its center and O atoms at the corners. The octahedra share edges and corners to give the crystal the best chemical composition (Figure 2.4) (Gupta and Tripathi, 2012). Brookite is considered complex as it has a larger cell volume and least dense compared to other two crystalline structures of TiO_2 and is not often used for experimental investigations (Thompson and Yates, 2007).
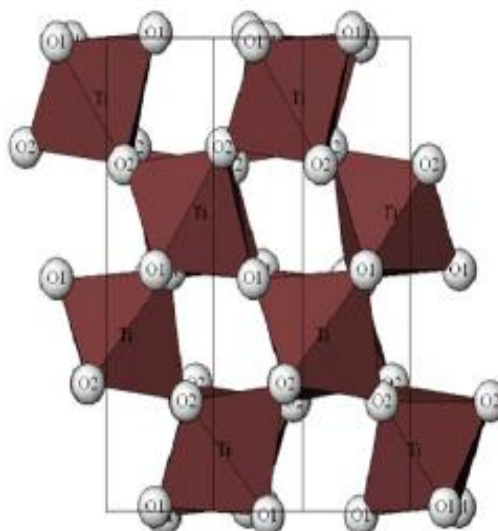
Figure 2.4: Crystal Structure of Brookite Phase TiO_2 (Gupta and Tripathi, 2012)

2.4.3 Anatase

The distortion of the TiO_6 octahedron is somewhat higher compared to rutile although anatase possesses the same tetragonal structure (Figure 2.5) (Simons and Dachille, 1967; Mo and Ching, 1995). It is found that at 0 K, anatase is more stable than rutile, however, there is only a small energy difference between the two phases (Muscat, Swamy and Harrison, 2002). The most active photocatalytically based on chemical properties, photocatalytic degradation of organic compounds and charge carrier dynamics is believed to be anatase. It forms intrinsic surface band bending naturally in deeper region with steeper potential compared to rutile (Figure 2.6) (Li et al., 2007). Therefore, surface hole trapping dominates as spatial charge separation is achieved by transfer of photogenerated holes towards surface of the particle through powerful upward band bending. Bulk recombination of electrons and holes happens in rutile so only holes which are closer to surface are trapped and transferred (Gupta and Tripathi, 2012).
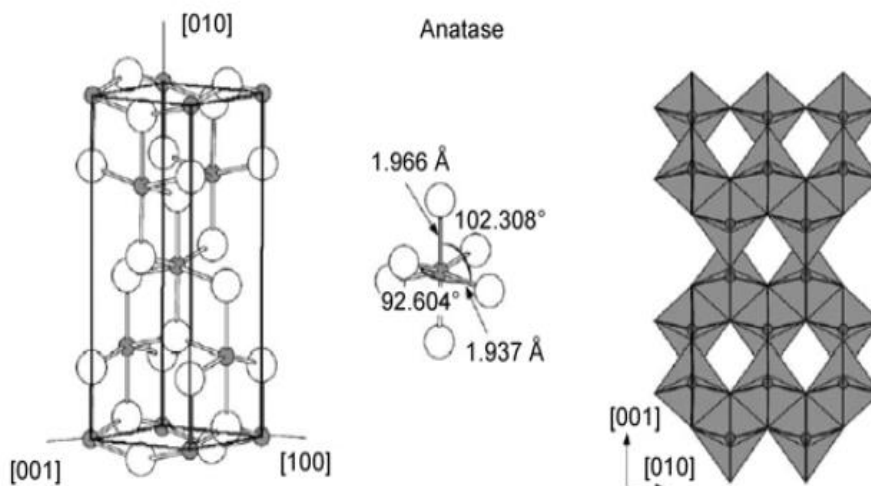
Figure 2.5: Crystal Structure of Anatase Phase TiO$_2$ (Gupta and Tripathi, 2012)
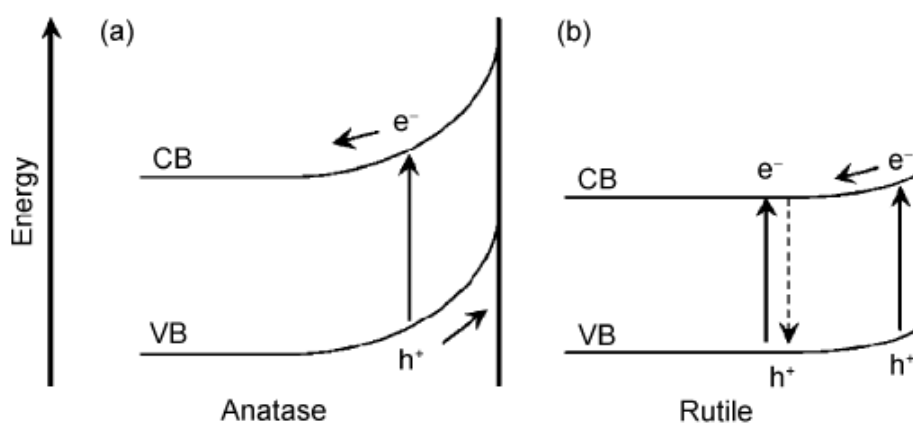
Figure 2.6: Surface Band Bending of Anatase and Rutile Phases of TiO$_2$ (Gupta and Tripathi, 2012)

2.5 TiO$_2$ Nanostructures

Many detailed research works opt to enhance the performances of the photocatalytic materials by targeting several important features related to TiO$_2$ nanostructures. TiO$_2$ nanostructures have huge surface area-to-volume ratio which enhance effective charge separation and trapping at the surface (Nagaveni et al., 2004). The opaqueness of TiO$_2$ nanostructures in light was proven to be able to enhance the oxidation capability in contrast to the bulky TiO$_2$ catalysts (Siddiquey et al., 2008). In other words, TiO$_2$ nanostructures show substantial development in terms of their chemical and physical properties. TiO$_2$ nanostructures can be fabricated in diverse morphologies such as

nanotubes, nanospheres (Nakata and Fujishima, 2012) and nanopores (Chong et al., 2010).

2.5.1   Nanospheres

TiO$_2$ nanospheres (Figure 2.7) have zero dimensionality. It possesses particularly huge surface area, huge pore capacity and pore size. These characteristics assist in enlarging the available surface area and mass transfer rate for adsorption of organic pollutant (Nakata and Fujishima, 2012). These characteristics enhance the light-harvesting capabilities because they intensify light used, allowing more light to access the interior (Kondo et al., 2008; Li et al., 2007). This makes them a good candidate other than photocatalysis but also in dye-sensitized solar cells (DSSC) (Kondo et al., 2008). Nanospheres are fabricated from titanium alkoxide like titanium tetraisopropoxide or titanium tetrabutoxide with a polymer to give its porous structure (Liu et al., 2011). The nanospheres obtained are able to undergo further treatment using hydrothermal method, producing porous structures (Nakata and Fujishima, 2012).
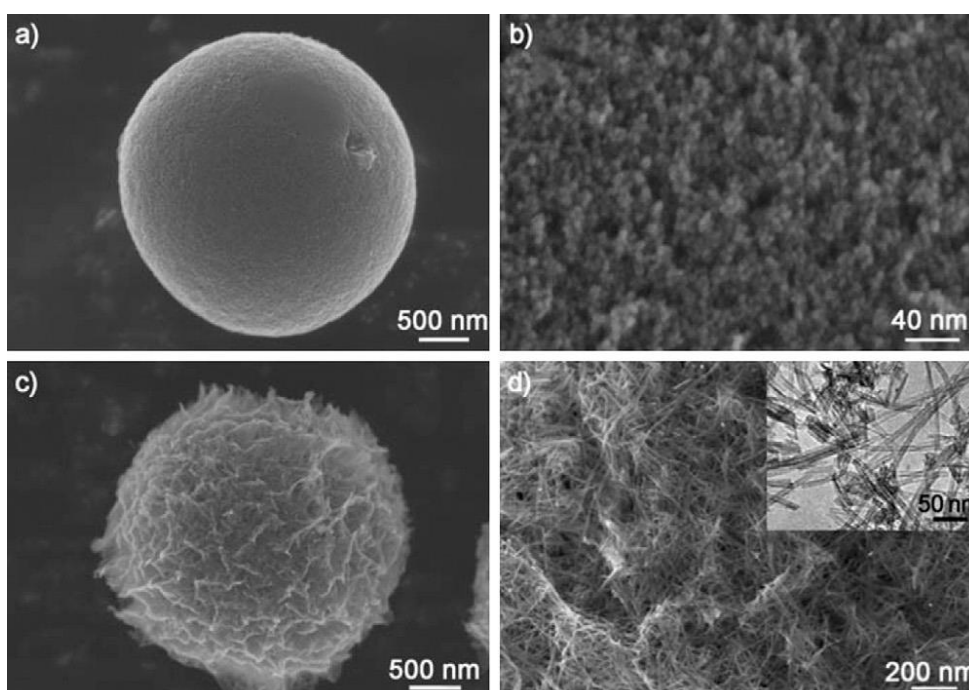
Figure 2.7: SEM and TEM Images of (a and b) TiO$_2$ Microspheres and (c and d) Hierarchical TiO$_2$ Microspheres (Zheng et al., 2010)

2.5.2   Nanotubes

TiO$_2$ nanotubes (Figure 2.8) are one-dimensional structures where the morphology and dimensions play a critical role in determining their performance in various photocatalytic applications. Nanotubes with larger surface-to-volume ratio allows faster interfacial charge carrier transfer rate and reduces the recombination rate of hole–electron (Almquist and Biswas, 2002). TiO$_2$ nanotubes can be fabricated by anodization. The structural characteristic of the formed nanotubes yields high photocatalytic decomposition since it allows diffusion of organic pollutants into TiO$_2$ nanotubes. Another attractive characteristic of nanotubes is its thin walls. The recombination of holes and electrons formed by photo-absorption are reduced due to these structural features. This is because the carrier diffusion length in TiO$_2$ is more than the thin walls of the nanotube. As a result, the possibility of TiO$_2$ nanotube arrays to have the potential to attain higher photocatalytic activity is high (Nakata and Fujishima, 2012).
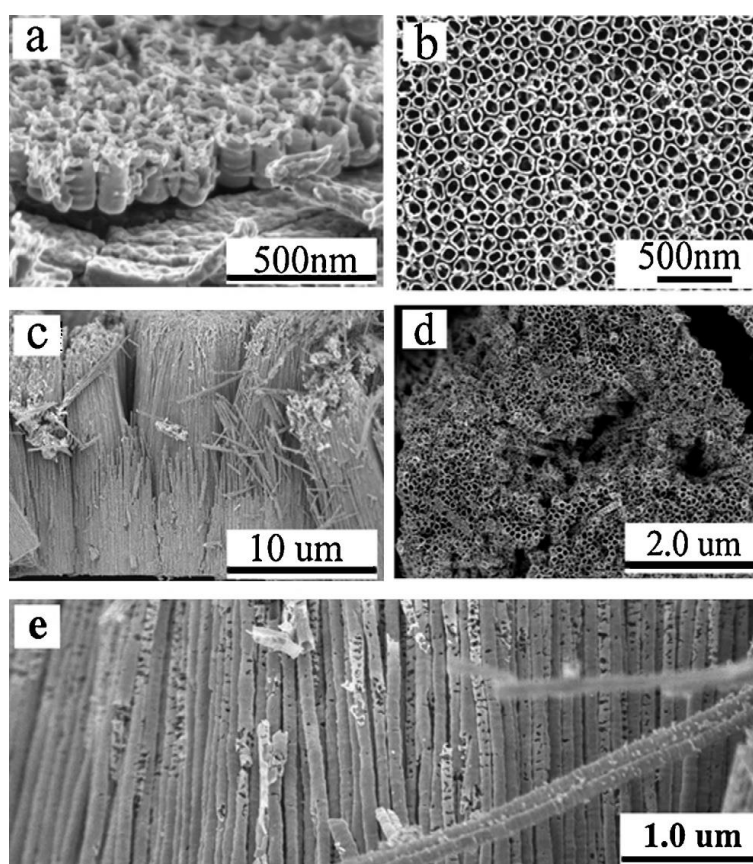
Figure 2.8: Cross-Sectional and Top View Images of TiO$_2$ Nanotube Arrays Prepared by Anodizing Ti Foil at 20 V in (a and b) 0.5 wt% HF Aqueous Solution for 20 min and in (c-e) Formamide Based Electrolyte for 6 hr (Liu et al., 2008)

2.5.3   Nanopores

Nanopores is popular in all kinds of fields especially in photocatalytic systems. There are various synthesis methods present for the formation of TiO_2 nanopores like sol–gel (Tomandl et al., 2000), evaporation (Tesfamichael et al., 2007), anodization (Sulka et al., 2010) and ion-beam synthesis (Komarov et al., 2005). Notable interest has grown in the synthesis of nanoporous TiO_2 due to favourable application as nano-devices in recent years (Kalantar-zadeh et al., 2009). Among all the nanostructures of TiO_2, nanoporous TiO_2 possesses attractive features such as nontoxicity, improving the ability of exchanging ion, safe for the environment, good photocatalytic properties and larger surface-to-volume ratio. Among fabrication methods for nanoporous TiO_2, electrochemical anodization is usually chosen. Anodization is straight forward, affordable and commonly used. The shape and size of nanopore arrays is also adjustable to preferable dimensions in anodization. Furthermore, anodization fabricates strong adherent nanoporous TiO_2 layer (Figure 2.9) (Indira et al., 2012).
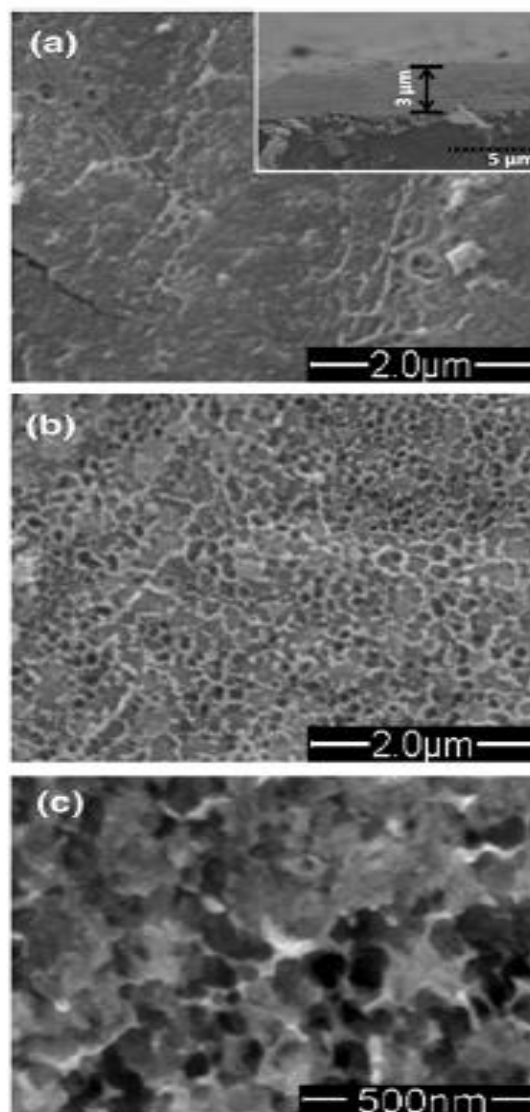
Figure 2.9: SEM Images of Nanoporous TiO$_2$ Anodized at 40 V in 0.13 M H$_2$SO$_4$ with Different HF Concentrations: (a) 0.1, (b) 0.15 and (c) 0.2 M (Indira et al., 2012)

2.6 Synthetization Methods of TiO$_2$ Structures

It has been found that photocatalytic properties of TiO$_2$ have strong reliance on surface morphology of TiO$_2$, such as huge surface area, huge pore capacity and size. In other words, the photocatalytic properties of TiO$_2$ also have direct relation with the formation methods (Nakata and Fujishima, 2012). There are a vast number of methods to synthesize TiO$_2$ such as hydrothermal synthesis (Xiao et al., 2006), sol-gel synthesis (Celik et al., 2007) and electrochemical anodization (Dikici et al., 2015).

2.6.1 Sol-Gel Method

Sol-gel synthesizes nanoparticles by tailoring the structure of primary precursor where metal atoms are distributed uniformly. It involves hydrolysis and polycondensation of a metal alkoxide, which eventually obtains hydroxide or oxide under certain conditions. The control of hydrolysis is essential to acquire homogeneous macromolecular oxide networks (Wu et al., 2002).

Sol–gel method begins with hydrolysis of alkoxide or halide precursor with subsequent condensation to the inorganic framework. Formation of TiO_2 from titanium (IV) alkoxide proceeds via an acid-catalyzed hydrolysis followed by condensation. The reactions shown in Figure 2.10 are comparable to alcoxolation, oxolation, and olation (Figure 2.11) (Chen and Mao, 2007). The involvement of each reaction is determined by the amount of water used during gelation procedure and their involvement controls the structure of the final gel. Hydrolysis rates are low under low concentration of H_2O, causing excess titanium alkoxide to prefer the formation of Ti–O–Ti chains through alcoxolation due to each Ti is aligned with four O atoms. Formation of Ti–O–Ti chains produces close packing three-dimensional polymeric skeletons (Lakshmi, Patrissi and Martin, 1997).

$$(RO)_3-Ti-O-R+H_2O \xrightarrow{H^+} (RO)_3-Ti-O-H+R-OH$$

$$2(RO)_3-Ti-O-H \longrightarrow (RO)_3-Ti-O-Ti-(OR)_3+H_2O$$
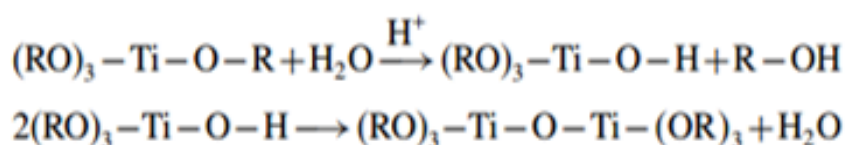
Sometimes, with alcoholic permutation reaction

$$Ti(OR)_3 + xR'(OH) \longleftrightarrow Ti(OR)_{3-x}(OR')_x + xROH$$

Figure 2.10: The Formation of TiO_2 from Titanium (IV) Alkoxide (Chen and Mao, 2007)

Alcoxolation:
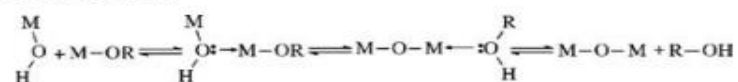
Oxolation:
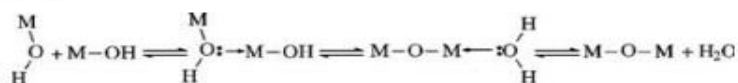
Olation:
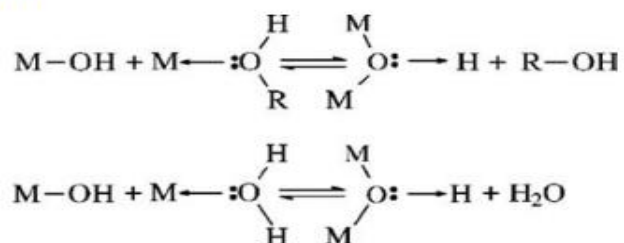
Figure 2.11: Alcoxolation, Oxolation, and Olation (Chen and Mao, 2007)

On the other hand, high hydrolysis rates favour the growth of $Ti(OH)_4$ and reduce relative contribution of alcoxolation with medium amount of H_2O. Presence of abundant Ti–OH and under developed three-dimensional polymeric skeletons causes the first order particles to be loosely packed. For high concentration of water, $Ti(OH)_4O+H_2$ is formed by coordinating water to $Ti(OH)_4$. It causes growth of polymeric Ti–O–Ti chains by olation. Overall, three-dimensionally developed gel skeleton obtains closely aligned first-order particles again. Ti–O+H–H formed are highly reactive and condense on other Ti–OH faster with production of water, gaining Ti–O–Ti chains (Lakshmi, Patrissi and Martin, 1997).

2.6.2 Hydrothermal Method

Hydrothermal process is performed under controlled pressure and temperature in an autoclaves (steel pressure vessel) with or without Teflon liners with the reaction in aqueous solutions. Internal pressure of the autoclave depends on the temperature and the amount of solution added. The temperature is allowed to exceed the boiling point of H_2O and reaching the pressure of vapour saturation. Hydrothermal method is known for preparing TiO_2 nanoparticles (Huang, 2008). For example, treatment of peptized precipitates of titanium precursor with H_2O can produce TiO_2 nanoparticles. The precipitates were made by mixing 0.5 M isopropanol solution of titanium butoxide into deionized water. It is then peptized at 70 °C for 1 hr in tetraalkylammonium hydroxides which acts as a peptizer. The as-prepared powders were washed using deionized water

and ethanol then dried at 60 °C after filtration and heat treated for 2h at 240 °C (Chen and Mao, 2007).

2.6.3   Anodization Method

Anodization has been broadly studied and proven to be able to produce various TiO_2 morphologies on Ti foils. Anodization can perform under self-organizing conditions and able to produce highly ordered arrays of closely packed vertically aligned nanopores when tuned (Li, Wan and Feng, 2009). Nanostructured TiO_2 layers can be fabricated with Ti in electrolytes with or without fluoride in anodization (Masahashi et al., 2009; Kuromoto, Simão and Soares, 2007).

Anodization can be conducted in two modes, either by potentiostat (constant voltage) or galvanostat (constant current). Both potentiostat and galvanostat are served to quantify, control the voltage or current intensity flowing through a reference electrode and a working electrode. In potentiostatic mode, voltage of working electrode is monitored at certain level as to reference electrode by regulating the current of counter electrode. On the contrary, the current flow between a working electrode and a counter electrode in galvanostatic mode is fixed at constant level. Potentiostatic anodisation is commonly applied due to its effectiveness in manipulating the interpore distance through potential (Hebert et al., 2000). In common practice, oxidising reaction takes place at the metal (working electrode) which is connected to positive terminal (anode). Inert materials like gold, carbon or platinum are widely used as the counter electrode (cathode). They are connected to the negative terminal in an electrochemical system.

Smooth TiO_2 surfaces affects its application in the photocatalytic oxidation technology as it has low photocatalytic efficiency. TiO_2 nanopores were formed to eliminate this problem due to their huge surface area and huge pore capacity (Mazzarolo et al., 2012). Crystalline nanoporous TiO_2 layers only can be formed by anodization. Nanostructures are naturally amorphous, however, it can be altered into crystalline phases by annealing (He et al., 2013). Its morphology is highly dependent on the anodization conditions such as concentration of electrolyte, type of electrolyte, applied voltage, time and pH (Masahashi et al., 2009). After annealing, the amorphous TiO_2 is altered to different crystalline phases such as rutile and anatase (Dikici et al., 2015). Other advantages of anodization include strong adhesion between the oxide

layer with substrate (Oh and Chi, 2012; Park, Shin and Song, 2007) and simple control of the surface morphology (Xie et al., 2012; Ohtsu, Komiya and Kodama, 2013).

2.6.3.1 Effect of Electrolyte Concentration on Nanostructure Growth

As discussed above, the crystalline structure of TiO_2 depends on the conditions of anodization such as the temperature, applied voltage and electrolyte concentration. According to research, formation and morphology of anodized titania in fluoride containing electrolytes are affected by the concentration of fluoride ions (Xie and Blackwood, 2010). The SEM micrographs and AFM topographs for anodized Ti in aqueous electrolyte (H_2SO_4) with different HF concentrations is shown in Figure 2.9 and Figure 2.12, respectively. It is shown when the concentration of fluoride increases to 0.15 M, clear pores was observed. On the other hand, when concentration of fluoride goes below or above 0.15 M, distorted images were observed due to strong dissolution of the oxide layer (Ohtsu, Komiya and Kodama, 2013).

On the other hand, Figure 2.13 and Figure 2.14 show the SEM micrographs and AFM topographs for Ti anodized in an organic electrolyte (glycerol) containing different HF concentrations. The results for both types of electrolytes were identical. At HF concentration of 0.1 and 0.2 M, no pores were seen, whereas at 0.15 M pores were observed. From the results above, pores were observed at concentration of 0.15 M HF which make it the optimum concentration. This proves that concentration of electrolyte is important in changing the pore morphology (Indira et al., 2012).
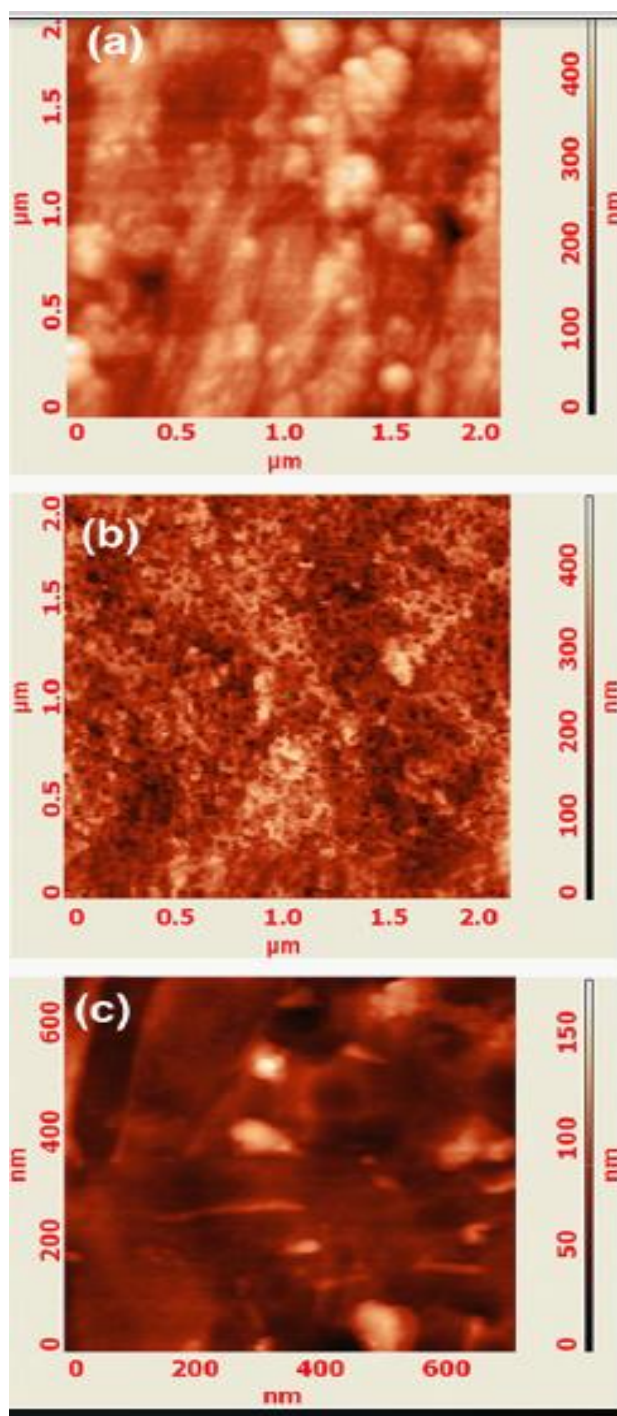
Figure 2.12: AFM topographies of the Ti Anodized at 40 V in 0.13 M H_2SO_4 with Different HF Concentrations: (a) 0.1, (b) 0.15 and (c) 0.2 M (Ohtsu, Komiya and Kodama, 2013)
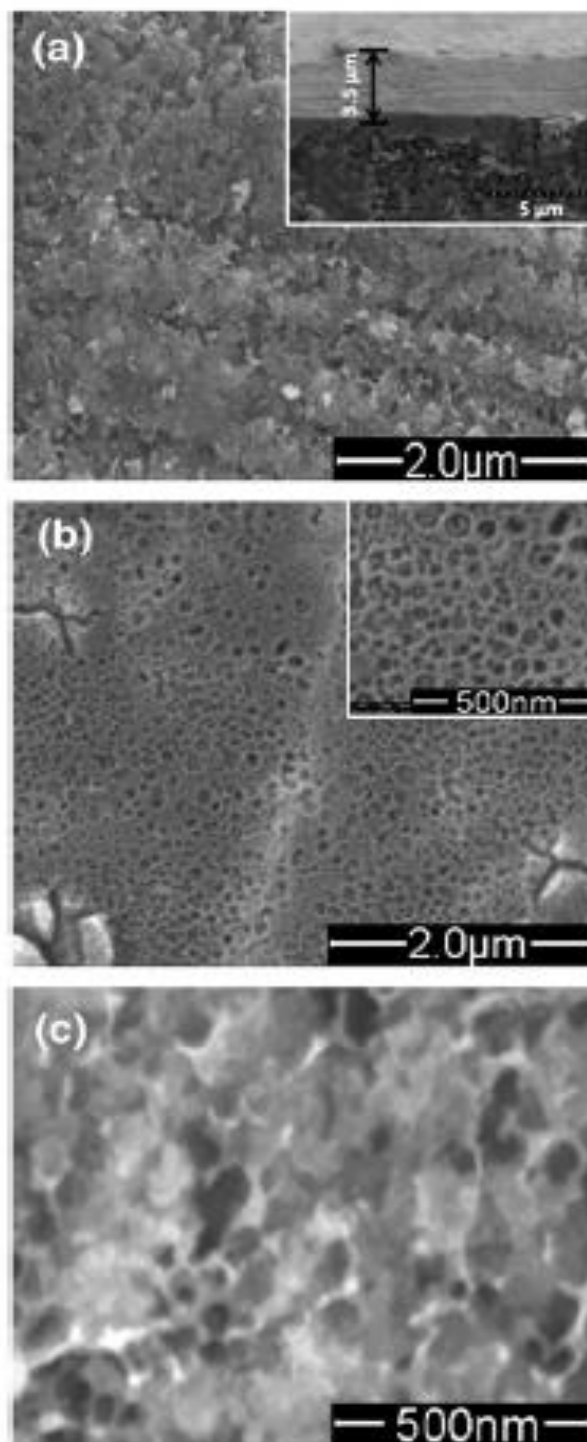
Figure 2.13: SEM Images of the Ti Anodized at 40 V in 0.13 M Glycerol with Different HF Concentrations: (a) 0.1, (b) 0.15 and (c) 0.2 M (Indira et al., 2012)
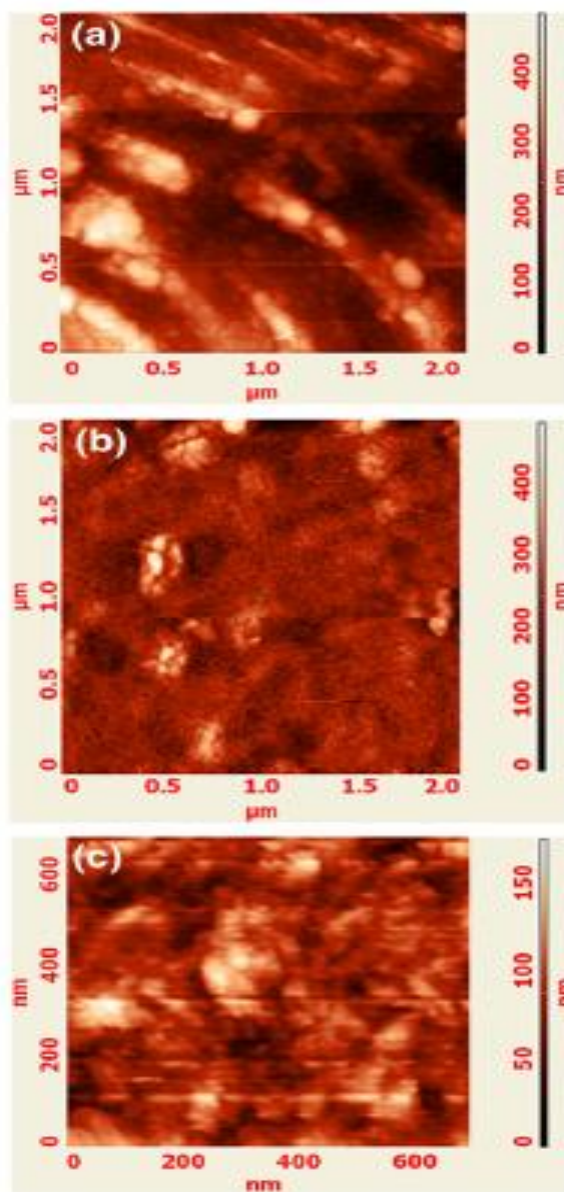
Figure 2.14: AFM Topographies of the Ti Anodized at 40 V in 0.13 M Glycerol with Different HF Concentrations: (a) 0.1, (b) 0.15 and (c) 0.2 M (Indira et al., 2012)

2.7   Summary

Photocatalytic process is meant to initiate particular reduction and oxidation (redox) reactions under irradiated semiconductors as a catalyst. Semiconductor catalysts has proved its efficiency in photocatalysis by degrading various types of ambiguous refractory organics to biodegradable compounds. The compounds are gradually mineralized to harmless CO_2 and H_2O. TiO_2 based photocatalysts were widely used to control environmental pollution. TiO_2 photocatalysis is a photo-induced charge separation that occurs on its surface and highly reactive O_2 species causes organic

mineralization and microbial inactivation without causing any secondary pollution. Different crystalline phases of TiO_2 which are rutile, anatase and brookite are able to be obtained after heat treatment. On the other hand, different methods such as sol-gel, anodization and hydrothermal can be used to synthesize TiO_2. Anodization method is more preferable as it can function under self-organizing conditions and able to produce highly ordered arrays of closely packed vertically aligned nanopores when tuned, which in this case, altering the concentration of electrolyte.

CHAPTER 3

METHODOLOGY AND WORK PLAN

3.1 Introduction

In this study, TiO_2 nanopore structures were grown using potentiostatic anodization. In a series of preliminary experiments, Ti was anodised in various concentration of ammonium fluoride (NH_4F) with the addition of ethylene glycol (EG) and potassium hydroxide (KOH). After sample preparation, the correlation among the morphological, structural and photocatalytic analysis of the samples were studied. Gantt charts were constructed to keep track on the progression of project.

3.2 Direct Anodic Growth of TiO_2 on Ti Foils

In this project, 0.1mm thick Ti foils with 99.5% purity were used as substrates. The Ti foil was cut into dimension of 4 cm x 1 cm. Before anodization, the foils were cleaned in ultrasonic bath containing acetone, ethanol and deionised water for 10 minutes respectively. The cleanliness of Ti foil is essential to make sure that all Ti substrates were free from debris, fingerprints and contaminants (Cai et al., 2005).

Anodization was performed in an electrochemical cell by connecting Ti foil to the positive terminal (anode) and a platinum foil to negative terminal (cathode), shown in Figure 3.1. The process was conducted at 50 V for 30 min in an electrolyte containing 99 ml of EG, 1 ml of KOH and different concentrations of NH_4F (0.1, 0.2, 0.3 and 0.4 g) with constant stirring. The foils were cleaned with deionized water after anodization. The annealing of anodized Ti foils was performed at 400 °C in a furnace for 2 h. Figure 3.2 summarises the synthesization procedure for the nanoporous TiO_2.
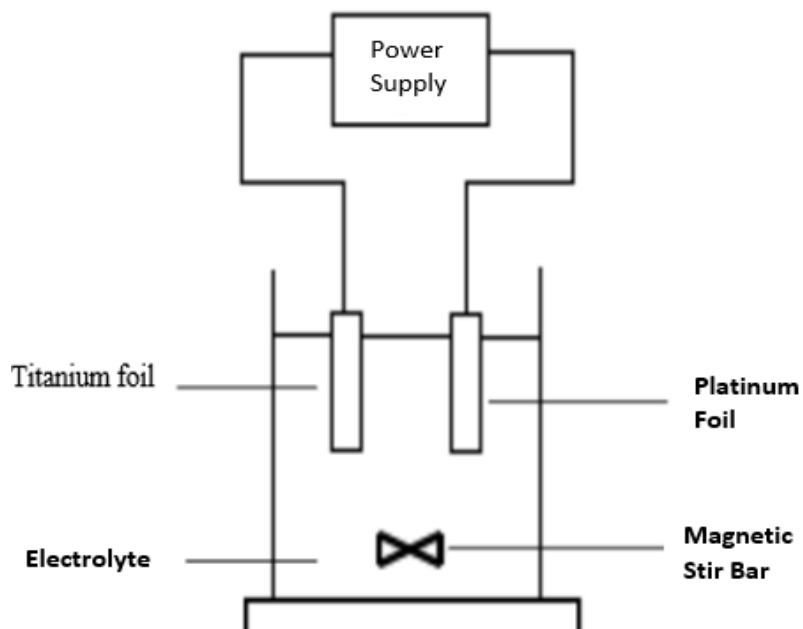
Figure 3.1: The Setup for Anodization Process
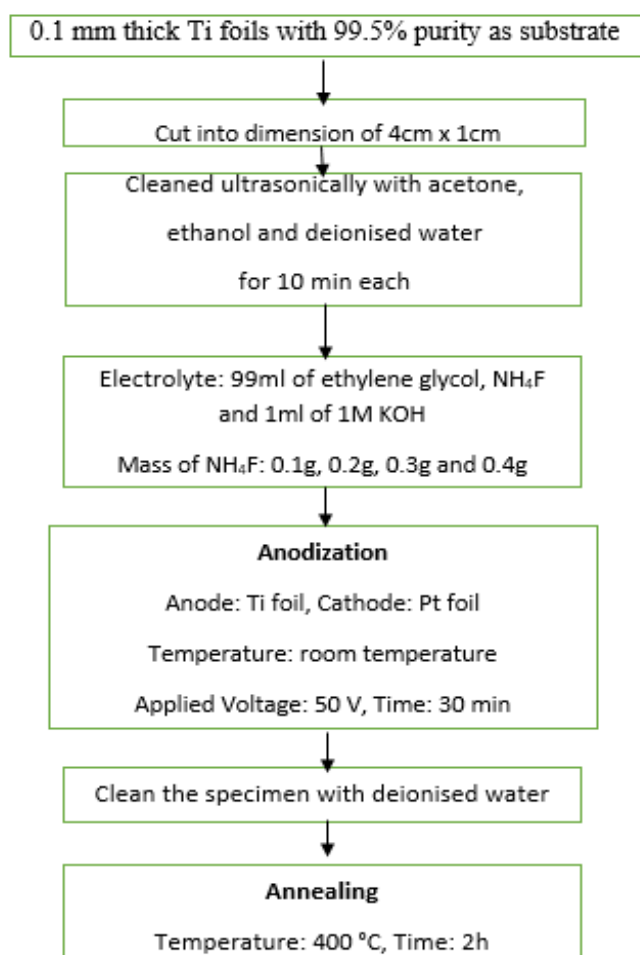
Figure 3.2: Flow Chart of the Synthesization Procedure for Nanoporous TiO_2

3.3   Sample Characterization

After TiO$_2$ nanopores have been prepared on substrates using various electrolyte concentrations, characterisations were conducted to analyse the morphological, structural and photocatalytic properties of the samples. The characterisation analysis is divided into three main parts, which are morphological, structural and photocatalytic analyses.

3.3.1   Morphological Analysis

The presence of the TiO$_2$ nanostructures were observed by using scanning electron microscope (SEM, Zeiss EVO 40). Then, the morphologies of anodic TiO$_2$ nanostructures were examined by field emission scanning electron microscope (FESEM, Jeol JSM-6701F, Japan). Samples were prepared by placing the samples on a sample holder using a carbon tape. The pore size and pore wall thickness of anodic TiO$_2$ nanostructures were measured using ImageJ software.

3.3.2   Structural Analysis

Energy-dispersive X-ray spectroscopy (EDX, Apollo X, Ametek Inc.) analysis was performed to verify the formation of oxide after anodization. The phases exist in the specimen were evaluated by X-ray diffraction (XRD, Siemens D5000 with Cu Kα radiation, $\lambda = 0.15406$ nm). The XRD analysis was conducted in the range of $2\theta = 20$–$80°$, where θ represents the angle between the scattering plane and the incident x-ray.

3.3.3   Photocatalytic Analysis

Figure 3.3 shows the set up for the photocatalytic analysis. The analysis is carried out using a setup involving MB solution along with an UV light source (PHILIPS, PLL 36W/10 4PIN). MB precursor powder used for the solution preparation is used without further purification. The MB solution of 35 ml was stored in beakers with TiO$_2$ catalysts submerged in it. The TiO$_2$ was placed under the light source with a gap about 200 mm for 5 h. A sample was also prepared to record its catalyst-free degradation as an arbitrator. The absorbance was measured with a UV–visible spectrophotometer (UV-Vis, Agilent, Cary 100).
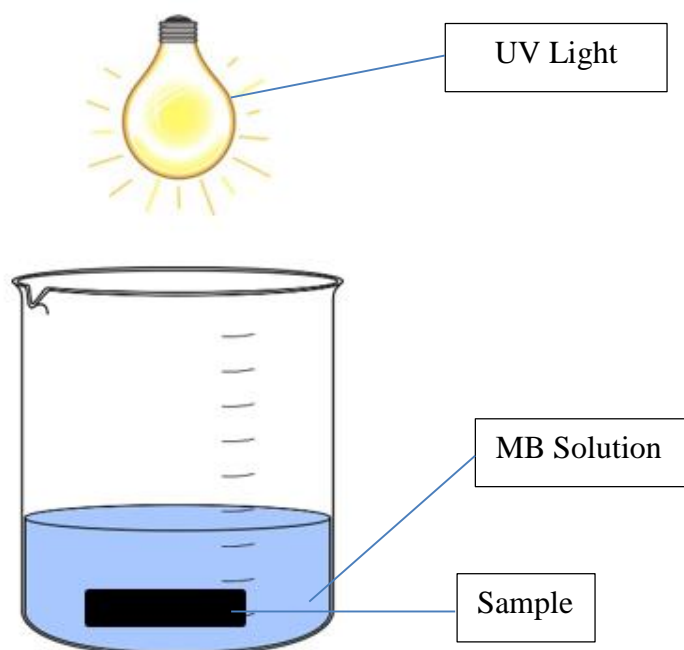
Figure 3.3: Schematic Diagram of Photocatalytic Process

3.4 Project Timeline

Table 3.1: Gantt Chart Part 1

No.	Project Activities	W1	W2	W3	W4	W5	W6	W7	W8	W9	W10	W11	W12	W13	W14
M1	Introduction	■	■	■											
M2	Literature Review				■	■	■	■	■						
M3	Research Methodology										■	■	■		
M4	Report Writing	■	■	■	■	■	■	■	■	■	■	■	■	■	■

Table 3.2: Gantt Chart Part 2

No.	Project Activities	W1	W2	W3	W4	W5	W6	W7	W8	W9	W10	W11	W12	W13	W14
M1	- Synthesize samples - Test samples with SEM - Anneal samples	■	■	■	■										
M2	Characterize samples with XRD, FESEM and EDX					■	■	■	■	■					
M3	Photocatalytic analysis on samples										■	■	■		
M4	Report Writing	■	■	■	■	■	■	■	■	■	■	■	■	■	■

3.5 Summary

In this project, TiO_2 nanopore structures were fabricated by anodization in different concentrations of electrolyte by altering the amount of NH_4F and then convert the nanopores to crystalline structures by annealing. After preparing the TiO_2 nanopores, characterisations were performed to analyse morphological, structural and photocatalytic properties of the samples. Morphologies were observed using SEM and FESEM, structural properties by EDX and XRD and photocatalytic properties by UV-Vis. Gantt charts were used to keep track on project to make sure the project can be completed on time.

CHAPTER 4

RESULTS AND DISCUSSIONS

4.1   Introduction

In this chapter, the results obtained from the films anodised in electrolyte at various concentrations of NH_4F (0.1, 0.2, 0.3 and 0.4 g) were discussed. The discussions include the morphological (SEM and FESEM), structural (EDX and XRD) and photocatalytic (UV-Vis) analyses on the samples.

4.2   Morphological Analysis

The effects of electrolyte concentration on the morphology of the samples were investigated by performing FESEM characterisation on the samples. Before FESEM, the presence of the nanopores were first observed by using SEM. Figure 4.1 shows the surface morphologies of the films anodized in different concentration of NH_4F. Based on Figure 4.1 (a), no pores were formed due to the absence of fluoride (F) ions. On the other hand, nanopores were successfully formed when the samples were anodized in 0.1-0.4 g of NH_4F as shown in Figure 4.1 (b-e). The sample anodized using 0.5 g of NH_4F shown in Figure 4.1 (f) did not show any presence of pores as well due to high chemical dissolution by F ions.
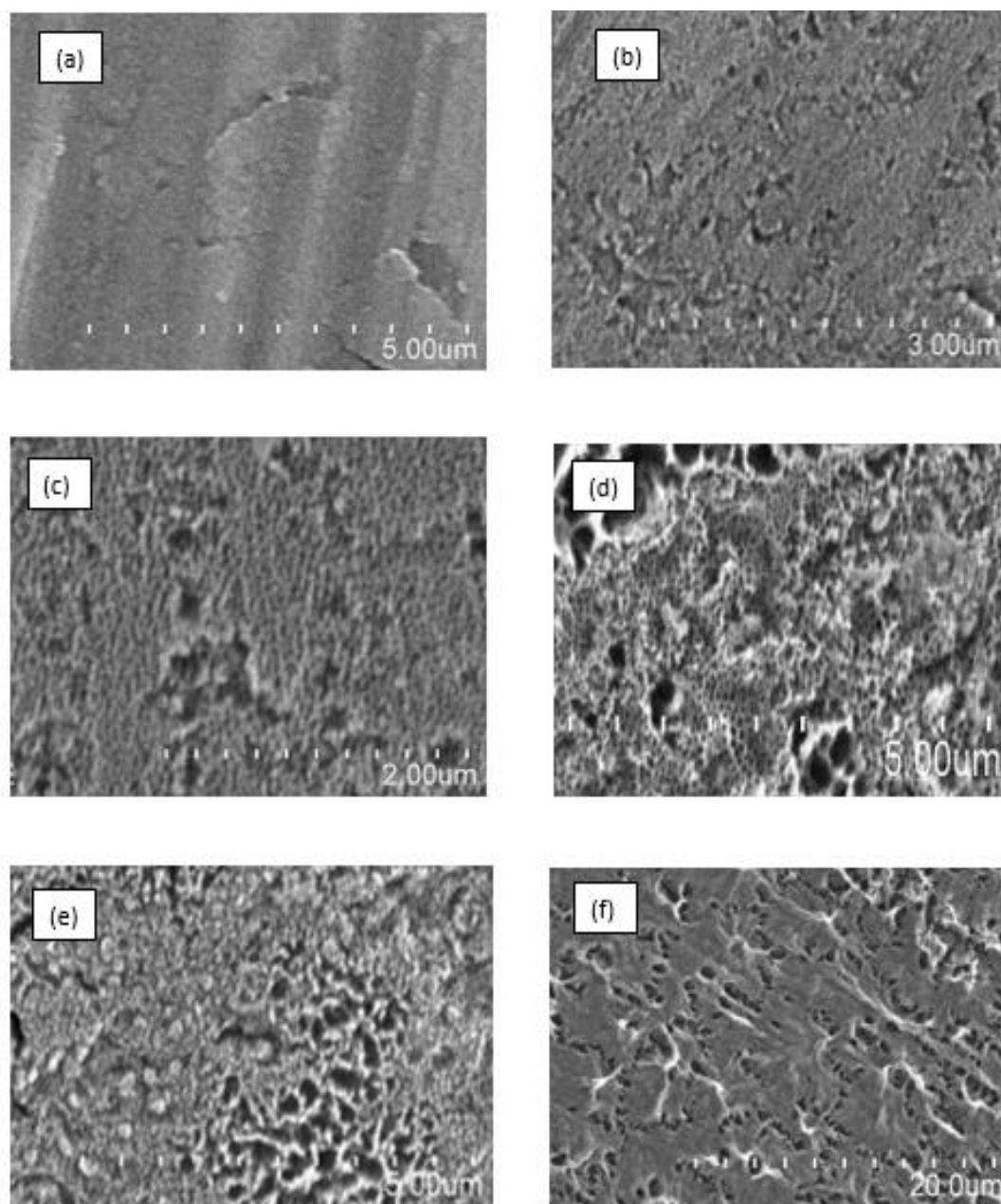
Figure 4.1: SEM Images of TiO$_2$ After Anodizing in (a) 0, (b) 0.1, (c) 0.2, (d) 0.3, (e) 0.4 and (f) 0.5 g of NH$_4$F, Ethylene glycol and KOH

After confirming the presence of nanopores on the samples, FESEM characterization was performed on the samples to observe the dimension of pores. Figure 4.2 shows the surface morphologies of the samples before and after anodization. Before the anodization, the Ti substrate had a flat surface which is shown in Figure 4.2 (a). After anodization, clear nanoporous structures were successfully formed as shown in Figure 4.2 (b-e).
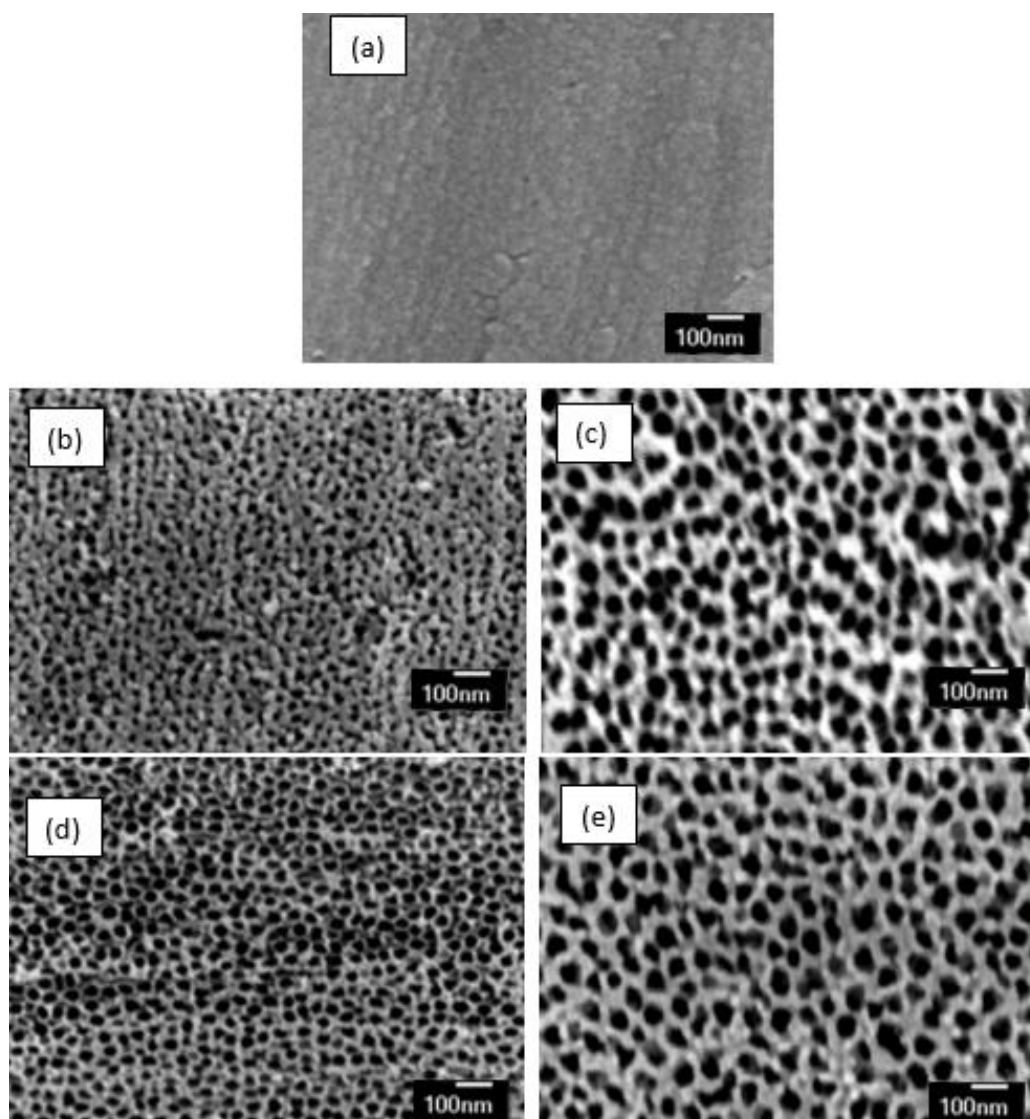
Figure 4.2: FESEM Images of (a) Film Before Anodization and Films After Anodizing in (b) 0.1, (c) 0.2, (d) 0.3 and (e) 0.4 g of NH_4F, Ethylene glycol and KOH

By using the FESEM images (Figure 4.2), the pore diameter and pore wall thickness were measured. Table 4.1 summarises the average pore diameter and pore wall thickness of the samples anodized with various concentration of NH_4F. Nanoporous TiO_2 anodized in 0.1 g of NH_4F (Figure 4.2 (b)) has an average pore diameter of ~12.4 nm and pore wall thickness of ~12.5 nm. The nanoporous TiO_2 prepared using 0.2 g of NH_4F (Figure 4.2 (c)) possesses an average pore diameter of ~27.6 nm and average pore wall thickness of ~8.7 nm. Nanoporous TiO_2 prepared using 0.3 g of NH_4F (Figure 4.2 (d)) showed a sudden decrease in average pore diameter (~21.7 nm) and pore wall thickness (~8.0 nm). By using 0.4 g of NH_4F (Figure 4.2 (e)), it showed a

slight increase on the readings with an average pore diameter of ~23.4 nm and average pore wall thickness of ~9.2 nm.

Table 4.1: Average Pore Diameter and Pore Wall Thickness of TiO_2 Films Fabricated Using Different Amount of NH_4F

Amount of NH₄F Added in The Electrolyte (g)	0.1g	0.2g	0.3g	0.4g
Average Pore Diameter (nm)	12.4	27.6	21.7	23.4
Average Pore Wall Thickness (nm)	12.5	8.7	8.0	9.2

Based on Table 4.1, it was found that both the pore diameter and pore wall thickness are dependent on the concentration of electrolyte. Nanoporous TiO_2 prepared using 0.3 g of NH_4F (Figure 4.2 (d)) shows more aligned nanoporous arrays compared to other samples as shown in Figure 4.2 (b), (c) and (e). Figure 4.2 (d) showed that the sample has the highest pore density and thinnest pore wall thickness. This statement is supported by the measurements shown in Table 4.1 where nanoporous TiO_2 prepared using 0.3 g of NH_4F has the thinnest average pore wall thickness of ~8.0 nm. It also has a smaller average pore diameter (~21.7 nm) based on the measurements. This compliments with the thin pore wall which increases the pore density.

4.3   Energy-Dispersive X-Ray Spectroscopy (EDX) Analysis

EDX analysis was conducted on the samples after anodization to analyse their chemical stoichiometry as shown in Figure 4.3. The inset in the Figure 4.3 shows the atomic and weight percentage of all elements. Significant Ti and O peaks are observed from the EDX spectrum indicates the formation of oxide layer after anodization. The atomic percentage of the Ti and O element are 66.69 % and 21.41 %, respectively. The ratio of atomic percentage for TiO_2 should be 1 for Ti and 2 for O based on its chemical formula. However, the result shows otherwise due to the detection of Ti substrate by EDX which contributes a spike in atomic percentage of Ti. Low amount of carbon (C), F and potassium (K) elements are also detected from the sample but in an almost negligible amount (0.53-8.23 at%). These trace elements are from the precursors (EG, NH_4F and KOH) used to synthesize nanoporous TiO_2.
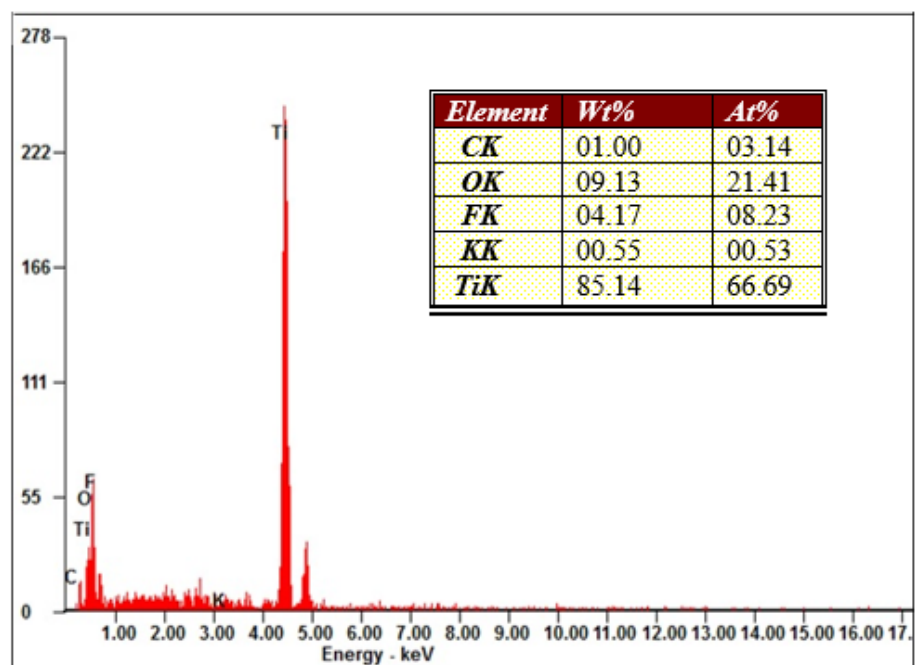
Figure 4.3: EDX Spectrum of the Nanoporous TiO_2 After Anodizing in 0.4 g of NH_4F, Ethylene glycol and KOH

4.4   X-Ray Diffraction Analysis (XRD)

XRD analysis was conducted on the samples to analyse the phases existing in the samples. Figure 4.4 shows the XRD patterns of films with and without annealing. The as-prepared sample (without annealing) is amorphous and only Ti peaks were detected. On the other hand, the formation of crystalline structures of anatase were detected from the annealed films regardless of their electrolyte concentrations.
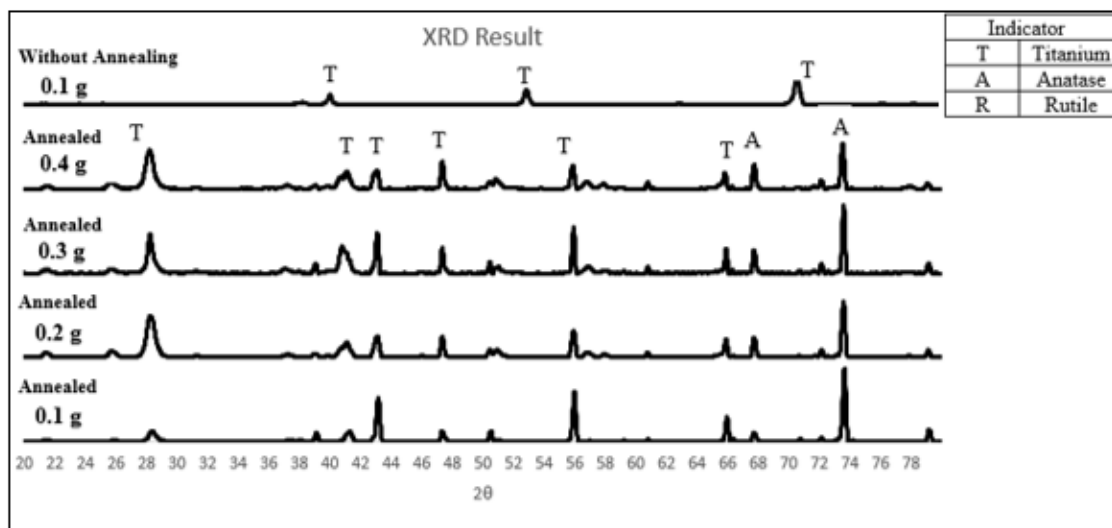
Figure 4.4: XRD Patterns of Film Without Annealing (Anodized in 0.1 g of NH₄F) and Annealed Films Anodized in Different Electrolyte Concentration

Based on the XRD patterns of annealed films (Figure 4.4), anatase peaks are found at 67.7 and 73.6 $^{\circ}$ (ICDD no. 01-070-8501), corresponding to (116) and (215), respectively. The most abundant peaks are Ti peaks found in 28.3, 41.3, 43.1, 47.3, 56.0 and 65.9 $^{\circ}$ (ICDD no. 00-046-1238), corresponding to $(\bar{2}02)$, $(\bar{2}03)$, (003), $(\bar{6}02)$, $(\bar{2}04)$ and $(\bar{2}23)$, respectively. It is shown that the annealed sample anodized with 0.3 g of NH₄F has the highest intensity of anatase peaks among all samples.

4.5   Photocatalytic Analysis

Photocatalytic analysis was conducted on the samples to determine their efficiency as a photocatalyst. Photocatalytic activity of the samples was evaluated by the degradation rate of methylene blue (MB) solutions under UV light illumination for a period of time. The absorbance values of the samples were measured using UV-Vis spectrometer at the maximum absorption wavelength of MB which is 668 nm.

Figure 4.5 shows the degradation rate of MB against time. The degradation rate of the sample without anodization is trivial due to its low photocatalytic efficiency of approximately 5%. On the other hand, all samples that have gone through anodization showed better photocatalytic efficiencies, regardless of the concentration of anodization electrolyte. This proves that anodization is crucial for producing nanoporous TiO₂ layers to increase their photocatalytic efficiency as mentioned in Section 2.6.3.
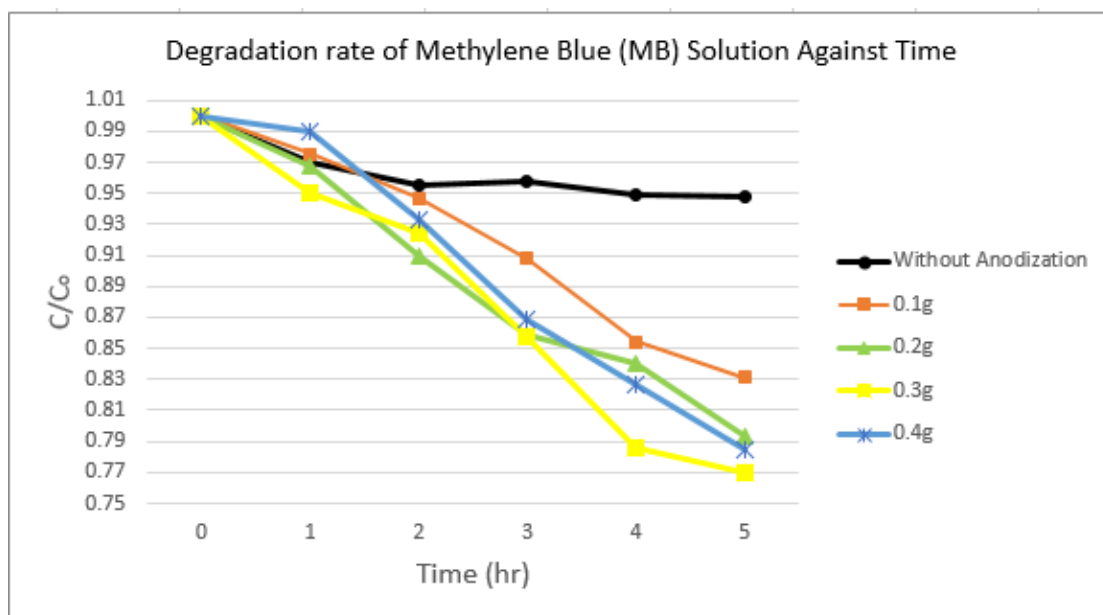
Figure 4.5: Degradation Rate of MB Solution Against Time by Film Before Anodization and Films After Anodizing in Various Concentrations of NH₄F, Ethylene glycol and KOH

The sample anodized by using 0.3 g of NH₄F showed the best photocatalytical performance with an efficiency of ~23%. This result can be explained by referring to Figure 4.2 (d), where the sample anodized with 0.3 g of NH₄F has the best pore morphology and aligned nanoporous arrays compared to others. The sample has the highest pore density (small pore diameter and thinnest pore wall thickness) as shown in Table 4.1. These characteristics increased its surface-to-volume ratio which increased the absorbance of dye and thus increased the degradation rate of the MB solution.

Referring to Figure 4.4, it is found that all annealed samples contained crystalline structures (anatase). The annealed sample anodized with 0.3 g of NH₄F has showed the highest intensity of anatase peaks. Besides, the sample also has narrower anatase peaks compared to others. Yu and Wang (2010) states that the higher intensity of the peaks reflects that the fabricated nanoparticles are crystalline and narrower peaks specify large crystallite size. Gupta and Tripathi (2011) states that to achieve high photocatalytic activity the TiO₂ nanostructures must attain two characteristics which are large surface area for absorbing substrates and high crystallinity to minimize the rate of photoexcited e^-/h^+ recombination, explained in Section 2.3.1. From the results obtained from Figure 4.2 and 4.4, the sample anodized by using 0.3 g of NH₄F

fulfilled both of the requirements. Therefore, it showed the best photocatalytical performance among all samples.

4.6 Summary

The results of morphological (SEM and FESEM), structural (EDX and XRD) and photocatalytic (UV-Vis) analyses on the samples anodised in electrolytes with various concentrations of NH_4F (0.1 g, 0.2 g, 0.3 g and 0.4 g) were discussed in this chapter. Based on the morphological analysis (SEM), it is shown that only samples anodized in 0.1-0.4 g of NH_4F have nanoporous structures. On the other hand, FESEM shows that TiO_2 prepared using 0.3 g of NH_4F has the thinnest average pore wall thickness of ~8.0 nm and small average pore diameter (~21.7 nm). EDX analysis shows significant Ti and O peaks, which indicates the formation of oxide layer after anodization. From the XRD analysis, annealed sample anodized with 0.3 g of NH_4F once again stood out from the other samples by having the highest intensity of anatase peaks. Finally, photocatalytic analysis was performed on the samples and TiO_2 prepared using 0.3 g of NH_4F displays the best photocatalytic performance based on the characteristics above.

CHAPTER 5

CONCLUSIONS AND RECOMMENDATIONS

5.1 Conclusions

TiO_2 nanopores were successfully grown on Ti substrate anodized in electrolyte consists of 0.1, 0.2, 0.3 and 0.4 g of ammonium fluoride (NH_4F) with the addition of ethylene glycol (EG) and potassium hydroxide (KOH). The concentration of electrolyte has noticeable effects on the morphological, structural, as well as the photocatalytic properties of the nanopores. XRD analysis showed the presence of crystalline TiO_2 structures (anatase) after annealing. From the results, it was discovered that the optimum concentration of electrolyte to fabricate nanoporous TiO_2 is by adding 0.3 g of NH_4F into EG and KOH. This is because of its large surface-to-volume ratio (pore diameter (~21.7 nm) and thin pore wall (~8 nm)) and high crystallinity of anatase peaks which enhances its photocatalytic performance (~23%).

5.2 Recommendations for future work

Based on current research, the recommendations listed for future research works are as following:

i. Photoelectrochemical analysis can be performed on the samples for photocurrent measurement under UV light to determine the light harvesting efficiency of the samples.

ii. Use petri dish with lid made out of high purity quartz as a container for methylene blue (MB) and TiO_2 film during photocatalysis because it is resistant to stain, scratch and heat. It also has high transparency range, especially to UV light.

REFERENCES

Ali, G., Chen, C., Yoo, S., Kum, J. and Cho, S. (2011). Fabrication of complete titania nanoporous structures via electrochemical anodization of Ti. *Nanoscale Research Letters*, 6(1), p.332.

Almquist, C. and Biswas, P. (2002). Role of Synthesis Method and Particle Size of Nanostructured TiO_2 on Its Photoactivity. *Journal of Catalysis*, 212(2), pp.145-156.

Anpo, M. (2017). *Preparation, Characterization, and Reactivities of Highly Functional Titanium Oxide-Based Photocatalysts Able to Operate under UV–Visible Light Irradiation: Approaches in Realizing High Efficiency in the Use of Visible Light*.

Banerjee, A., Joo, S. and Min, B. (2012). Photocatalytic Degradation of Organic Dye by Sol-Gel-Derived Gallium-Doped Anatase Titanium Oxide Nanoparticles for Environmental Remediation. *Journal of Nanomaterials*, 2012, pp.1-14.

Bard, A. (1979). Photoelectrochemistry and heterogeneous photo-catalysis at semiconductors. *Journal of Photochemistry*, 10(1), pp.59-75.

Blanco, J., Malato, S., de las Nieves, J., Ferna´ndez, P., 2001. Method of sedimentation of colloidal semiconductor particles, European patent application EP-1-101-737-A1, European Patent Office Bulletin 21.

Bonnet, M., Massard, C., Veisseire, P., Camares, O. and Awitor, K. (2015). Environmental Toxicity and Antimicrobial Efficiency of Titanium Dioxide Nanoparticles in Suspension. *Journal of Biomaterials and Nanobiotechnology*, 06(03), pp.213-224.

Cai, Q., Paulose, M., Varghese, O. and Grimes, C. (2005). The Effect of Electrolyte Composition on the Fabrication of Self-Organized Titanium Oxide Nanotube Arrays by Anodic Oxidation. *Journal of Materials Research*, 20(01), pp.230-236.

Celik, E., Keskin, I., Kayatekin, I., Ak Azem, F. and Özkan, E. (2007). Al_2O_3–TiO_2 thin films on glass substrate by sol–gel technique. *Materials Characterization*, 58(4), pp.349-357.

Chen, X. and Mao, S. (2007). Titanium Dioxide Nanomaterials: Synthesis, Properties, Modifications, and Applications. *ChemInform*, 38(41).

Choi, J., Ryu, S., Balcerski, W., Lee, T. and Hoffmann, M. (2008). Photocatalytic production of hydrogen on $Ni/NiO/KNbO_3/CdS$ nanocomposites using visible light. *Journal of Materials Chemistry*, 18(20), p.2371.

Chong, M., Jin, B., Chow, C. and Saint, C. (2010). Recent developments in photocatalytic water treatment technology: A review. *Water Research*, 44(10), pp.2997-3027.

Curco, D., Gime´nez, J., Addarak, A., Cervera-March, S., Esplugas, S., 2002. Effects of radiation absorption and catalyst concentration on the photocatalytic degradation of pollutants. Catal. Today 76, 177-188.

Dikici, T., Yildirim, S., Yurddaskal, M., Erol, M., Yigit, R., Toparli, M. and Celik, E. (2015). A comparative study on the photocatalytic activities of microporous and nanoporous TiO$_2$ layers prepared by electrochemical anodization. *Surface and Coatings Technology*, 263, pp.1-7.

Fujihira, M., Satoh, Y. and Osa, T. (1981). Heterogeneous photocatalytic oxidation of aromatic compounds on TiO$_2$. *Nature*, 293(5829), pp.206-208.

FUJISHIMA, A. and HONDA, K. (1972). Electrochemical Photolysis of Water at a Semiconductor Electrode. *Nature*, 238(5358), pp.37-38.

FUJISHIMA, A., ZHANG, X. and TRYK, D. (2008). TiO$_2$ photocatalysis and related surface phenomena. *Surface Science Reports*, 63(12), pp.515-582.

Gupta, S. and Tripathi, M. (2011). A review of TiO$_2$ nanoparticles. *Chinese Science Bulletin*, 56(16), pp.1639-1657.

Gupta, S. and Tripathi, M. (2012). A review on the synthesis of TiO$_2$ nanoparticles by solution route. *Open Chemistry*, 10(2).

Hagfeldt, A. and Graetzel, M. (1995). Light-Induced Redox Reactions in Nanocrystalline Systems. *Chemical Reviews*, 95(1), pp.49-68.

Harikishore, M., Sandhyarani, M., Venkateswarlu, K., Nellaippan, T. and Rameshbabu, N. (2014). Effect of Ag Doping on Antibacterial and Photocatalytic Activity of Nanocrystalline TiO2. *Procedia Materials Science*, 6, pp.557-566.

HEBERT, K. R., LILLARD, R. S. & MACDOUGALL, B. R. Oxide Films: Proceedings of the International Symposium. 2000. The Electrochemical Society.

He, G., Xie, L., Yin, G., Liao, X., Zou, Y., Huang, Z., Yao, Y., Chen, X. and Wang, F. (2013). Synthesis and mechanism of (101)-preferred orientation rutile titania via anodic spark oxidation. *Surface and Coatings Technology*, 228, pp.201-208.

Hernández-Alonso, M., Fresno, F., Suárez, S. and Coronado, J. (2009). Development of alternative photocatalysts to TiO$_2$: Challenges and opportunities. *Energy & Environmental Science*, 2(12), p.1231.

Huang, X. (2008). *Nanotechnology research*. 1st ed. New York: Nova Science Publishers, p.106.

Hwang, D., Kim, H., Lee, J., Kim, J., Li, W. and Oh, S. (2005). Photocatalytic Hydrogen Production from Water over M-Doped La$_2$Ti$_2$O$_7$(M = Cr, Fe) under Visible Light Irradiation ($\lambda > 420$ nm). *The Journal of Physical Chemistry B*, 109(6), pp.2093-2102.

Indira, K., Ningshen, S., Mudali, U. and Rajendran, N. (2012). Effect of anodization parameters on the structural morphology of titanium in fluoride containing electrolytes. *Materials Characterization*, 71, pp.58-65.

Jang, J., Kim, H. and Lee, J. (2012). Heterojunction semiconductors: A strategy to develop efficient photocatalytic materials for visible light water splitting. *Catalysis Today*, 185(1), pp.270-277.

Kalantar-zadeh, K., Sadek, A., Partridge, J., McCulloch, D., Li, Y., Yu, X., Spizzirri, P. and Wlodarski, W. (2009). Nanoporous titanium oxide synthesized from anodized Filtered Cathodic Vacuum Arc Ti thin films. *Thin Solid Films*, 518(4), pp.1180-1184.

Komarov, F., Vlasukova, L., Milchanin, O., Gaiduk, P., Yuvchenko, V. and Grechnyi, S. (2005). Ion-beam formation of nanopores and nanoclusters in SiO2. *Vacuum*, 78(2-4), pp.361-366.

Kondo, Y., Yoshikawa, H., Awaga, K., Murayama, M., Mori, T., Sunada, K., Bandow, S. and Iijima, S. (2008). Preparation, Photocatalytic Activities, and Dye-Sensitized Solar-Cell Performance of Submicron-Scale TiO2Hollow Spheres. *Langmuir*, 24(2), pp.547-550.

Krengvirat, W., Sreekantan, S., Noor, A., Kawamura, G., Muto, H. and Matsuda, A. (2013). Single-step growth of carbon and potassium-embedded TiO2 nanotube arrays for efficient photoelectrochemical hydrogen generation. *Electrochimica Acta*, 89, pp.585-593.

Kuromoto, N., Simão, R. and Soares, G. (2007). Titanium oxide films produced on commercially pure titanium by anodic oxidation with different voltages. *Materials Characterization*, 58(2), pp.114-121.

Lakshmi, B., Patrissi, C. and Martin, C. (1997). Sol−Gel Template Synthesis of Semiconductor Oxide Micro- and Nanostructures. *Chemistry of Materials*, 9(11), pp.2544-2550.

Lee, S. and Park, S. (2013). TiO$_2$ photocatalyst for water treatment applications. *Journal of Industrial and Engineering Chemistry*, 19(6), pp.1761-1769.

Li, G., Chen, L., Graham, M. and Gray, K. (2007). A comparison of mixed phase titania photocatalysts prepared by physical and chemical methods: The importance of the solid–solid interface. *Journal of Molecular Catalysis A: Chemical*, 275(1-2), pp.30-35.

Li, H., Bian, Z., Zhu, J., Zhang, D., Li, G., Huo, Y., Li, H. and Lu, Y. (2007). Mesoporous Titania Spheres with Tunable Chamber Stucture and Enhanced Photocatalytic Activity. *Journal of the American Chemical Society*, 129(27), pp.8406-8407.

Li, J., Wan, L. and Feng, J. (2009). Micro arc oxidation of S-containing TiO$_2$ films by sulfur bearing electrolytes. *Journal of Materials Processing Technology*, 209(2), pp.762-766.

Linsebigler, A., Lu, G. and Yates, J. (1995). Photocatalysis on TiO$_2$ Surfaces: Principles, Mechanisms, and Selected Results. *Chemical Reviews*, 95(3), pp.735-758.

Liu, B., Nakata, K., Sakai, M., Saito, H., Ochiai, T., Murakami, T., Takagi, K. and Fujishima, A. (2011). Mesoporous TiO$_2$ Core–Shell Spheres Composed of Nanocrystals with Exposed High-Energy Facets: Facile Synthesis and Formation Mechanism. *Langmuir*, 27(13), pp.8500-8508.

Liu, Z., Zhang, X., Nishimoto, S., Murakami, T. and Fujishima, A. (2008). Efficient Photocatalytic Degradation of Gaseous Acetaldehyde by Highly Ordered TiO$_2$ Nanotube Arrays. *Environmental Science & Technology*, 42(22), pp.8547-8551.

Macák, J., Tsuchiya, H. and Schmuki, P. (2005). High-Aspect-Ratio TiO$_2$ Nanotubes by Anodization of Titanium. *Angewandte Chemie International Edition*, 44(14), pp.2100-2102.

Masahashi, N., Mizukoshi, Y., Semboshi, S. and Ohtsu, N. (2009). Enhanced photocatalytic activity of rutile TiO$_2$ prepared by anodic oxidation in a high concentration sulfuric acid electrolyte. *Applied Catalysis B: Environmental*, 90(1-2), pp.255-261.

Mazzarolo, A., Lee, K., Vicenzo, A. and Schmuki, P. (2012). Anodic TiO$_2$ nanotubes: Influence of top morphology on their photocatalytic performance. *Electrochemistry Communications*, 22, pp.162-165.

Mo, S. and Ching, W. (1995). Electronic and optical properties of three phases of titanium dioxide: Rutile, anatase, and brookite. *Physical Review B*, 51(19), pp.13023-13032.

Muscat, J., Swamy, V. and Harrison, N. (2002). First-principles calculations of the phase stability of TiO$_2$. *Physical Review B*, 65(22).

Nagaveni, K., Sivalingam, G., Hegde, M. and Madras, G. (2004). Photocatalytic Degradation of Organic Compounds over Combustion-Synthesized Nano-TiO$_2$. *Environmental Science & Technology*, 38(5), pp.1600-1604.

Nakata, K. and Fujishima, A. (2012). TiO$_2$ photocatalysis: Design and applications. *Journal of Photochemistry and Photobiology C: Photochemistry Reviews*, 13(3), pp.169-189.

Nyein, N., Lockman, Z., Matsuda, A., Kawamura, G., Tan, W. and Oo, T. (2016). *Formation of TiO$_2$ nanotube arrays in KOH added fluoride-ethylene glycol (EG) electrolyte and its photoelectrochemical response*.

Oh, H. and Chi, C. (2012). Eu–N-doped TiO$_2$ photocatalyst synthesized by micro-arc oxidation. *Materials Letters*, 86, pp.31-33.

Ohtsu, N., Komiya, S. and Kodama, K. (2013). Effect of electrolytes on anodic oxidation of titanium for fabricating titanium dioxide photocatalyst. *Thin Solid Films*, 534, pp.70-75.

Padmanabhan, P.V.A., Sreekumar, K.P., Thiyagarajan, T.K., Satpute, R.U., Bhanumurthy, K., Sengupta, P., Dey, G.K., Warrier, K.G.K., 2006. Nano-crystalline titanium dioxide formed by reactive plasma synthesis. Vacuum 80, 11e12.

Park, Y., Shin, K. and Song, H. (2007). Effects of anodizing conditions on bond strength of anodically oxidized film to titanium substrate. *Applied Surface Science*, 253(14), pp.6013-6018.

Prabhu, S., Viswanathan, T., Jothivenkatachalam, K. and Jeganathan, K. (2014). Visible Light Photocatalytic Activity of CeO_2-ZnO-TiO_2Composites for the Degradation of Rhodamine B. *Indian Journal of Materials Science*, 2014, pp.1-10.

Sclafani, A., Palmisano, L. and Schiavello, M. (1990). Influence of the preparation methods of titanium dioxide on the photocatalytic degradation of phenol in aqueous dispersion. *The Journal of Physical Chemistry*, 94(2), pp.829-832.

Siddiquey, I., Furusawa, T., Sato, M., Honda, K. and Suzuki, N. (2008). Control of the photocatalytic activity of TiO_2 nanoparticles by silica coating with polydiethoxysiloxane. *Dyes and Pigments*, 76(3), pp.754-759.

Simons, P. and Dachille, F. (1967). The structure of TiO_2II, a high-pressure phase of TiO_2. *Acta Crystallographica*, 23(2), pp.334-336.

Sugiyama, K. and Takéuchi, Y. (1991). The crystal structure of rutile as a function of temperature up to 1600°C. *Zeitschrift für Kristallographie - Crystalline Materials*, 194(3-4).

Suh, K., Kang, J., Baek, J., Kim, T., Lee, J., Jeon, Y., Jang, M. and Kim, S. (2010). Efficacy of Ultraviolet A1 Phototherapy in Recalcitrant Skin Diseases. *Annals of Dermatology*, 22(1), p.1.

Sul, Y., Johansson, C., Jeong, Y. and Albrektsson, T. (2001). The electrochemical oxide growth behaviour on titanium in acid and alkaline electrolytes. *Medical Engineering & Physics*, 23(5), pp.329-346.

Sulka, G., Kapusta-Kołodziej, J., Brzózka, A. and Jaskuła, M. (2010). Fabrication of nanoporous TiO_2 by electrochemical anodization. *Electrochimica Acta*, 55(14), pp.4359-4367.

Tesfamichael, T., Motta, N., Bostrom, T. and Bell, J. (2007). Development of porous metal oxide thin films by co-evaporation. *Applied Surface Science*, 253(11), pp.4853-4859.

Thompson, T. and Yates, J. (2007). Surface Science Studies of the Photoactivation of TiO_2 — New Photochemical Processes. *ChemInform*, 38(1).

Tighineanu, A., Ruff, T., Albu, S., Hahn, R. and Schmuki, P. (2010). Conductivity of TiO_2 nanotubes: Influence of annealing time and temperature. *Chemical Physics Letters*, 494(4-6), pp.260-263.

Tomandl, G., Mangler, M., Pippel, E. and Woltersdorf, J. (2000). Evidence of nanopores in sol–gel based TiO_2 and TiN ultrafiltration membranes. *Materials Chemistry and Physics*, 63(2), pp.139-144.

Tsuchiya, H. and Schmuki, P. (2004). Thick self-organized porous zirconium oxide formed in H_2SO_4/NH_4F electrolytes. *Electrochemistry Communications*, 6(11), pp.1131-1134.

Venieri, D., Fraggedaki, A., Kostadima, M., Chatzisymeon, E., Binas, V., Zachopoulos, A., Kiriakidis, G. and Mantzavinos, D. (2014). Solar light and metal-doped TiO_2 to eliminate water-transmitted bacterial pathogens: Photocatalyst characterization and disinfection performance. *Applied Catalysis B: Environmental*, 154-155, pp.93-101.

Wu, M., Lin, G., Chen, D., Wang, G., He, D., Feng, S. and Xu, R. (2002). Sol-Hydrothermal Synthesis and Hydrothermally Structural Evolution of Nanocrystal Titanium Dioxide. *Chemistry of Materials*, 14(5), pp.1974-1980.

Viessman Jr., W., Hammer, M.J., 1998. Water Supply and Pollution Control, sixth ed. Addison Wesley Longman Inc, California USA.

Xiao, J., Peng, T., Li, R., Peng, Z. and Yan, C. (2006). Preparation, phase transformation and photocatalytic activities of cerium-doped mesoporous titania nanoparticles. *Journal of Solid State Chemistry*, 179(4), pp.1161-1170.

Xie, L., Liao, X., Xu, H., Yin, G., Huang, Z., Yao, Y., Chen, X. and Gu, J. (2012). A facile one-step anodization treatment to prepare multi-level porous titania layer on titanium. *Materials Letters*, 72, pp.141-144.

Xie, Z. and Blackwood, D. (2010). Effects of anodization parameters on the formation of titania nanotubes in ethylene glycol. *Electrochimica Acta*, 56(2), pp.905-912.

Yu, J. and Wang, B. (2010). Effect of calcination temperature on morphology and photoelectrochemical properties of anodized titanium dioxide nanotube arrays. *Applied Catalysis B: Environmental*, 94(3-4), pp.295-302.

Zhang, L. and Yu, J. (2003). A sonochemical approach to hierarchical porous titania spheres with enhanced photocatalytic activity Electronic Supplementary Information (ESI) available: XRD patterns, nitrogen adsorption/desorption isotherms, pore size distribution curves, photocatalytic activities and physicochemical properties of HPT and SMT. See http://www.rsc.org/suppdata/cc/b3/b306013f/. *Chemical Communications*, (16), p.2078.

Zhao, L., Chang, J. and Zhai, W. (2005). Effect of Crystallographic Phases of TiO_2 on Hepatocyte Attachment, Proliferation and Morphology. *Journal of Biomaterials Applications*, 19(3), pp.237-252.

Zheng, Z., Huang, B., Qin, X., Zhang, X. and Dai, Y. (2010). Strategic Synthesis of Hierarchical TiO_2 Microspheres with Enhanced Photocatalytic Activity. *Chemistry - A European Journal*, 16(37), pp.11266-11270.

Zhou, S., Ding, X. and Wu, L. (2013). Fabrication of ambient-curable superhydrophobic fluoropolysiloxane/TiO_2 nanocomposite coatings with good mechanical properties and durability. *Progress in Organic Coatings*, 76(4), pp.563-570.

Zou, Z., Ye, J., Sayama, K. and Arakawa, H. (2001). Direct splitting of water under visible light irradiation with an oxide semiconductor photocatalyst. *Nature*, 414(6864), pp.625-627.